Volume 17

Journal of Biomedical Engineering Society of India

Medical & Life sciences Engineering

June 2023

CONTENT			
Sl.No	**Author Name**	**Title of Paper**	**Page Number**

A Tree-based Machine Learning Decision Support System for detecting Polycystic Ovarian Syndrome

Varada Vivek Khanna [1], Krishanaraj Chadaga [2], Niranajana Sampathila[3], Srikanth Prabhu[4]

[1]Khanna: Department of Biomedical engineering,
Manipal Institute of Technology,
Manipal, Karnataka, 576104, India.
Varada.khanna@learner.manipal.edu

[3] Sampathila: Department of Biomedical engineering
Manipal Institute of Technology,
Manipal, Karnataka, 576104, India.
niranjana.s@manipal.edu

[2]Chadaga: Department of Computer Science and Engineering
Manipal Institute of Technology,
Manipal, Karnataka, 576104, India
krishnaraj.chadaga1@learner.manipal.edu

[4]Prabhu: Department of Computer Science and Engineering
Manipal Institute of Technology,
Manipal, Karnataka, 576104, India
srikanth.prabhu@manipal.edu

Abstract:

Polycystic Ovarian Syndrome (PCOS) is a hormonal disorder that causes excessive production of Androgens in women during their reproductive years. PCOS manifests externally as obesity, excessive hair growth, acne, and internally as enlarged ovaries due to cysts formation. Misdiagnosis or underdiagnosis at an early stage puts the patient at high risk of total infertility, cardiovascular issues, and type-II diabetes. Artificial Intelligence (AI) has revolutionized healthcare and is actively contributing to technological advancements in Medicine. Machine Learning (ML), a subset of AI, has extensively influenced disease screening and diagnosis automation. This study creates and evaluates multiple ML tree-based pipelines to detect PCOS. The best-performing architecture was for the Light GBM classifier producing an accuracy of 98%. Further, a layer of explainable AI with Shapley additive explanations (SHAP) is augmented to interpret this pipeline. With this research, we aim to build a reliable and meaningful architecture to assist a medical professional in detecting PCOS.

Keywords: *Explainable Artificial Intelligence; Machine Learning; Polycystic Ovarian Syndrome; Shapley additive explanations*

I. INTRODUCTION

Polycystic Ovarian Syndrome (PCOS) is an endocrine disorder that has become a prevalent women Public Health issue. Globally, 5.5% to 12.6% of women in their childbearing years suffer from PCOS **[1].** PCOS is primarily characterized by anovulation, clinical hyperandrogenism, and polycystic ovaries. Androgens are considered male sex hormones, but in small amounts, these hormones assist the efficient functioning of a women's reproductive system. With the excessive increase of androgens, various manifestations of PCOS, such as hirsutism, male-pattern baldness, oligomenorrhea, excessive oil production, and infertility, can be observed **[2-3]**. The exact cause of PCOS remains to be unknown. However, researchers have linked PCOS with genetic, lifestyle, and environmental factors **[4]**. Patients with this syndrome show symptoms of obesity, if not treated early, could lead to severe cardiovascular complications.

Machine Learning, a subset of Artificial Intelligence (AI), predominantly contributes to medical technological developments. Automation in disease detection, drug delivery, prognosis, triaging, and optimization of resources is possible because of the advent of ML **[5-7]**. Multiple studies propose an automated diagnosis of PCOS with a Machine Learning algorithm. Bharati et al. (2020) **[8]** built a PCOS diagnosis ML model. They utilized an open-source Kaggle repository with data from 541 fertile PCOS patients having 43 parameters **[9]**. An exhaustive comparison was presented between the deployed ML algorithms, such as Gradient boosting, Random Forest (RF), Logistic Regression (LR), and an RF-LR hybrid. The hybrid model achieved the highest accuracy of 91.01% with a recall of 90%. A Local Interpretable Model-Agnostic Explanations (LIME) based PCOS risk prediction model was developed by ÇİÇEK et al. (2021) **[10].** A similar earlier open-source dataset was utilized based on which the

LIME model explained the Random Forest classifier. RF provided an accuracy of 86.03% and a sensitivity of 85.37%. Operating on the same Kaggle dataset above, Hdaib et al. (2022) **[11]** created multiple algorithms deploying K-nearest Neighbors, Neural Networks, Naïve Bayes, Support Vector Machine, Logistic Regression, Linear Discriminant, and Classification Tree. On evaluation, Linear Discriminant outperformed other models with an accuracy and precision of 92.6% and 97.6%, respectively.

This study is an extension of our prior research on PCOS**,** where tree-based models like Random Forest and XGBoost performed exceptionally well compared to multiple ensembles and deep-learning classifiers **[12].** We have created tree-based models like Random Forest, XGBoost, Light GBM, and Catboost to obtain the best-performing algorithm to detect PCOS. Tree-based models are widely used for their high performance, stability, and robustness. These effectively map the non-linear relationship between the features and the target and can sometimes outperform complex neural networks.

The upcoming sections are Section 2, wherein data pre-processing and various models are explored; Section 3 encompasses the results and discussions; and the final section contains the conclusion of this study.

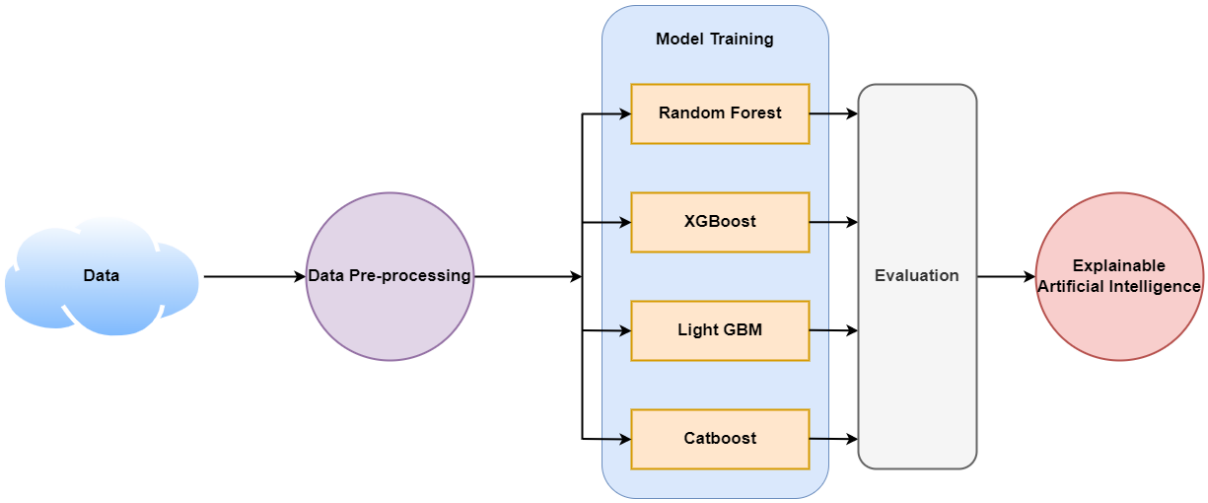

Figure 1: Workflow of the study

II. METHODS AND METHODOLOGY

2.1 Data description

This data utilized in the research was an open-source dataset from the Kaggle repository **[9]**. This dataset consisted of 541 fertile patients with 43 recorded attributes. This data was gathered from 10 different hospitals in Kerala. The data had 177 PCOS-positive. Out of the recorded 43 parameters, 24 were non-invasive features.

2.2 Data pre-processing

During data pre-processing, the feature statistical median replaced the missing values. Mutual Information performed feature engineering on the data. In Mutual Information, the correlation between the feature and target is calculated using the entropy measure. Further, the top 10 most significant features were manually extracted. The features were: Follicle No. (L), Follicle No. (R), Skin darkening (Y/N), hair growth(Y/N), Weight gain(Y/N), Fast food (Y/N), Cycle length(days), FSH/LH, AMH(ng/mL), and Cycle(R/I). A ratio of 80:20 was used to divide the data. 80% of the data would be used to train the classifiers, and the remaining 20% would validate the models. Data standardization was executed with the StandardScalar () function. As mentioned above, the PCOS-negative cases were severely lower than the PCOS-positive cases. This imbalance in the data can hinder the efficient training of the classifier. The classifier is likely to produce multiple False-Negatives, reducing the classifier's

reliability. Borderline Synthetic Minority Oversampling Technique (SMOTE) alleviated the imbalance observed in the target class. Both PCOS positive and negative classes now had 364 samples each.

2.3 Model training

The pre-processed data was used to train the tree-based classifiers: Random Forest, XGBoost, Light GBM, and Catboost. GridSearchCV assisted in the usage of the optimum hyperparameters. These Tree-based models have supervised learning algorithms that entail a series of conditional nodes that successively partition the data to make a prediction. Table 1 indicates the hyperparameters selected for each model.

Machine Learning Classifier	Best Parameter Specifications
Random Forest	{'bootstrap': True, 'max_depth': 80, 'max_features': 2, 'min_samples_leaf': 4, 'min_samples_split': 12, 'n_estimators': 300}
XGBoost	{'colsample_bytree': 0.3, 'gamma': 0.1, 'learning_rate': 0.05, 'max_depth': 3, 'min_child_weight': 1}
Light GBM	{'lambda_l1': 1, 'lambda_l2': 1, 'min_data_in_leaf': 30, 'num_leaves': 31, 'reg_alpha': 0.1}
Catboost	{'border_count': 5, 'depth': 3, 'iterations': 250, 'l2_leaf_reg': 3, 'learning_rate': 0.03}

III. RESULTS AND DISCUSSIONS

This section compares various performance metrics of the tree-based models to obtain the best-performing model for PCOS detection. The explainable AI technique SHAP will also be used to interpret the best-performing model.

3.1 Model evaluation

Metrics like accuracy, precision, recall, F-1 scores, AUC-ROC scores, Mathew's Correlation Coefficient, and Hamming loss are used to evaluate the performance. A high-performing model will have accuracy, precision, and recall values close to 100%. Ideally, these models will have F1-score, AUC-ROC scores, and Mathew's Correlation Coefficient close to 1. The hamming loss for such model will be almost 0. Table 2 indicates the performance metrics for the four models. Figure 2 depicts the AUC plots for the trained classifiers.

Table 2: Performance metric for the tree-based models along with comparison of a few previously conducted studies

Models	Random Forest	XGBoost	Light GBM	Catboost	[8]	[10]	[11]	[12]
Accuracy	0.97	0.95	0.98	0.95	0.91	0.86	0.90	0.98
Precision	0.97	0.95	0.97	0.94	-	-	0.89	0.97
Recall	0.95	0.92	0.98	0.95	0.9	0.83	0.90	0.98
F1-score	0.96	0.94	0.98	0.95	-	-	-	0.98
AUC-ROC score	0.99	0.99	1.00	1.00	-	-	-	1.00
Hamming Loss	0.03	0.05	0.02	0.05	-	-	-	-
Mathew's Correlation Coefficient	0.93	0.9	0.96	0.90	-	-	-	-

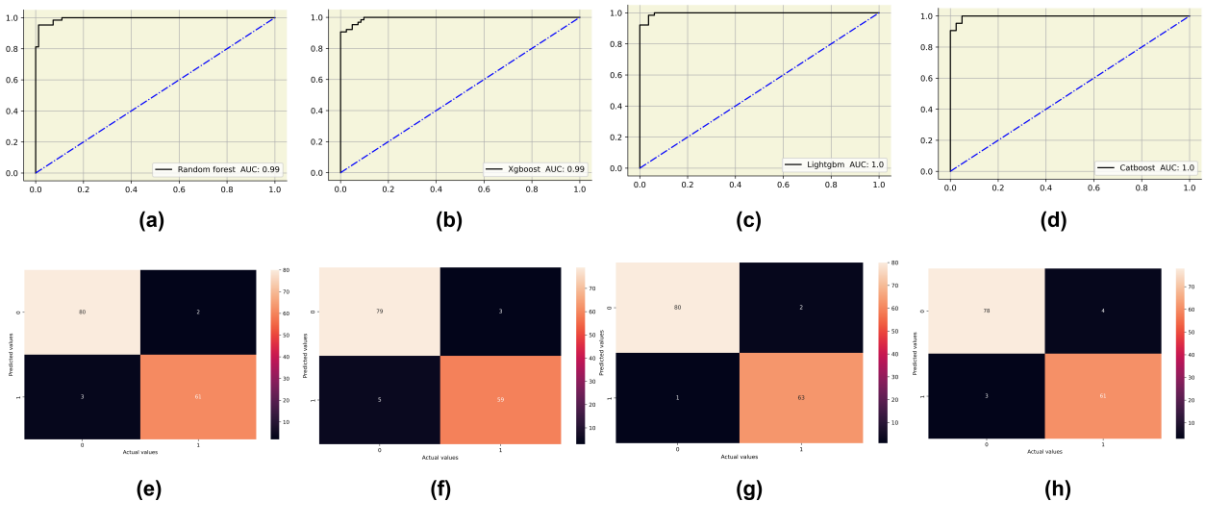

Figure 2: AUC plots and Confusion Metrics of the four tree-based models. Plots (a) and (e) correspond to Random Forest, plots (b) and (f) correspond to XGBoost, plots (c) and (g) correspond to Light GBM and plots (d) and (h) correspond to the Catboost classifier.

Light GBM has outperformed the remaining classifiers with accuracy, precision, and recall of 98%. This model has the lowest hamming loss value of 0.02. It had the highest true positives and just two false-negative samples. Random Forest had higher performance metrics than XGBoost and Catboost algorithms. Hence, we used SHAP to explain the prediction of the best tree-based model, Light GBM. The performance obtained for Light GBM is comparable to the best Stack-3 model in the prior study. This indicates that such tree-based models can outperform complex neural networks and various multi-level stacks.

3.2 Explainable Artificial Intelligence with SHAP

Shapley additive explanations are an extensive classifier explainable technique. This uses a game-theory approach and calculates the SHAP values for individual features based on their impact on the final prediction **[13]**. Figure 3 represents the SHAP plot and the feature importance plot of the best-performing algorithm, Light-GBM. The x-axis indicates the SHAP values, and the y-axis represents the features. The colors blue to red indicate a low to high feature value. Each dot on the plot represents a data sample. Here, a higher follicle number in the right ovary significantly impacts the prediction of PCOS. Should a patient face excessive hair growth, weight gain, skin darkening, and an irregular menstrual cycle, the Light GBM model will likely predict the patient as PCOS-positive. Further, more follicles in the left ovary contribute positively to PCOS prediction. These observations align with the PCOS research **[3]**.

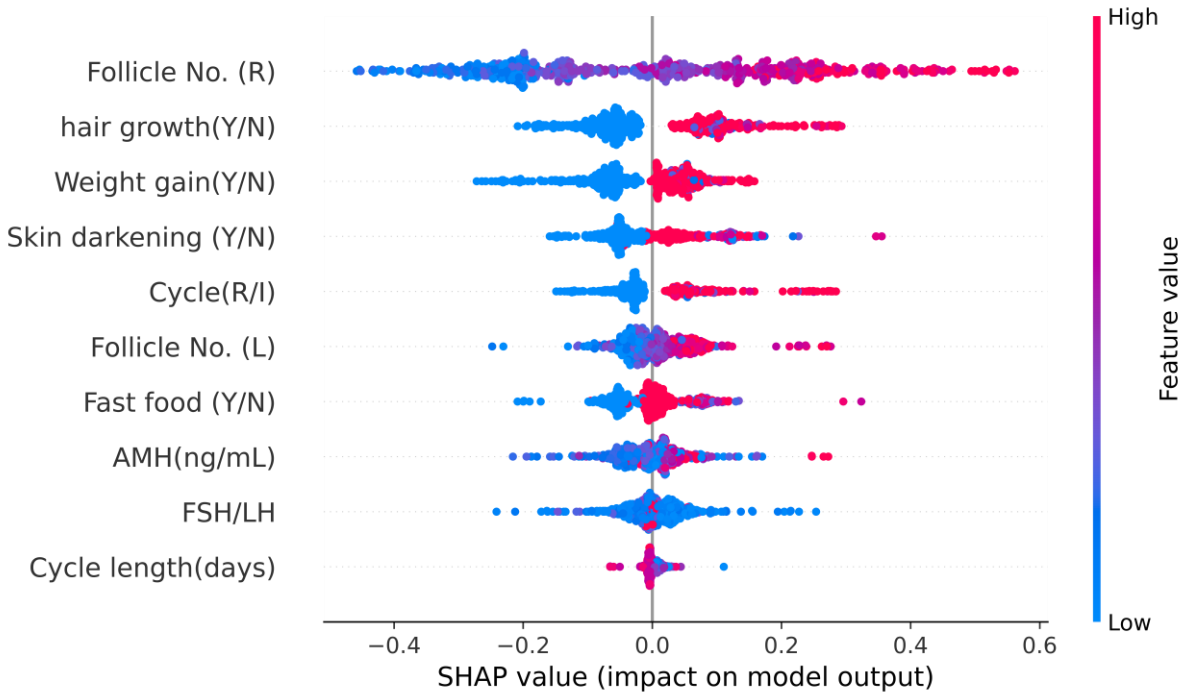

Figure 3: SHAP Beeswarm plot for understanding the Light GBM classifications.

IV. CONCLUSION

Polycystic Ovarian Syndrome is a prevalent women's health issue that often goes underdiagnosed or misdiagnosed. Failure to detect PCOS early on can lead to severe cardiovascular disorders, diabetes mellitus, and complete infertility. With the advent of machine learning, it is possible to automate detection and holistically consider all related parameters while making a prediction. In this study, we have advanced on a previously published PCOS study and observed the Light GBM algorithm outperforming all tree-based models. Additionally, a layer for model explainability is deployed for this classifier. We believe it is critical to alleviating the gaps in the domain of medicine and informatics so that the predictions made by a classifier are as meaningful to a medical professional as they would be to a Machine Learning expert.

REFERENCES

[1] Mehreen, T. S., Ranjani, H., Kamalesh, R., Ram, U., Anjana, R. M., & Mohan, V. (2021). Prevalence of polycystic ovarian syndrome among adolescents and young women in India. *Journal of Diabetology*, *12*(3), 319-325.

[2] Handelsman, D. J. (2020). Androgen physiology, pharmacology, use and misuse. *Endotext [Internet]*.

[3] Azziz, R. (2004). PCOS: a diagnostic challenge. *Reproductive biomedicine online*, *8*(6), 644-648.

[4] Ajmal, N., Khan, S. Z., & Shaikh, R. (2019). Polycystic ovary syndrome (PCOS) and genetic predisposition: A review article. *European journal of obstetrics & gynecology and reproductive biology: X*, *3*, 100060.

[5] Chadaga, K., Prabhu, S., Sampathila, N., Chadaga, R., KS, S., & Sengupta, S. (2022). Predicting cervical cancer biopsy results using demographic and epidemiological parameters: a custom stacked ensemble machine learning approach. *Cogent Engineering*, *9*(1), 2143040.

[6] Khanna, V. V., Chadaga, K., Sampathila, N., Prabhu, S., Chadaga, R., & Umakanth, S. (2022). Diagnosing COVID-19 using artificial intelligence: a comprehensive review. *Network Modeling Analysis in Health Informatics and Bioinformatics*, *11*(1), 25.

[7] He, S., Leanse, L. G., & Feng, Y. (2021). Artificial intelligence and machine learning assisted drug delivery for effective treatment of infectious diseases. *Advanced Drug Delivery Reviews*, *178*, 113922.

[8] Bharati, S., Podder, P., & Mondal, M. R. H. (2020, June). Diagnosis of polycystic ovary syndrome using machine learning algorithms. In *2020 IEEE Region 10 Symposium (TENSYMP)* (pp. 1486-1489). IEEE.

[9] https://www.kaggle.com/datasets/prasoonkottarathil/polycystic-ovary-syndrome-pcos?select=PCOS_data_without_infertility.xlsx assessed on 10th December 2022.

[10] ÇİÇEK, İ. B., KÜÇÜKAKÇALI, Z., & YAĞIN, F. H. (2021). Detection of risk factors of PCOS patients with Local Interpretable Model-agnostic Explanations (LIME) Method that an explainable artificial intelligence model. *The Journal of Cognitive Systems*, *6*(2), 59-63.

[11] Hdaib, D., Almajali, N., Alquran, H., Mustafa, W. A., Al-Azzawi, W., & Alkhayyat, A. (2022, May). Detection of Polycystic Ovary Syndrome (PCOS) Using Machine Learning Algorithms. In *2022 5th International Conference on Engineering Technology and its Applications (IICETA)* (pp. 532-536). IEEE.

[12] Khanna, V. V., Chadaga, K., Sampathila, N., Prabhu, S., Bhandage, V., & Hegde, G. K. (2023). A Distinctive Explainable Machine Learning Framework for Detection of Polycystic Ovary Syndrome. *Applied System Innovation*, *6*(2), 32.

[13] Lundberg, S. M., & Lee, S. I. (2017). A unified approach to interpreting model predictions. *Advances in neural information processing systems*, *30*.

Automated Oral Squamous Cell Carcinoma Detection from Histopathological Images using Deep Neural Networks

Tushar Nayak
Department of Biomedical Engineering
Manipal Academy Of Higher Education
Manipal, India
https://orcid.org/0000-0002-4328-7983

Dr. Niranjana Sampathila
Department of Biomedical Engineering
Manipal Academy Of Higher Education
Manipal, India
https://orcid.org/0000-0002-3345-360X

***Abstract*— Oral squamous cell carcinoma (OSCC) is a prevalent type of head and neck cancer that affects millions of people worldwide. The early detection and diagnosis of OSCC are crucial for improving patient outcomes and survival rates. In this paper, we propose the use of the Inceptionv3 deep learning model on a binary OSCC dataset with colour normalization, contrast enhancement, and unsharp masking techniques. The proposed method achieved an accuracy of 95.89% and an F1-score of 0.9569, demonstrating the potential of deep learning models in assisting pathologists in the early detection and diagnosis of OSCC.**

Keywords— oral cancer, digital histopathology, deep learning, transfer learning

I. INTRODUCTION

The most prevalent form of oral cancer accounting for nearly 90% [1] of all malignant oral cancers, Oral Squamous Cell Carcinoma (OSCC) is a malignant neoplasm of the oral cavity. It can arise from the cells around oral cavity including the lips, tongue, cheeks, gums and the palate. While it is a slow growing cancer that can go unnoticed in early stages, in later stages OSCC has proven to be invasive and aggressive. This has necessitated better diagnostic modalities that aid the existing modalities. On a global scale, OSCC is reported by the World Health Organization as being the eleventh most common cancer globally, with nearly three lakh new cases and one lakh death in the year 2020 alone [2][3]. While the incidence of OSCC can vary from country to country, the work conducted by the Global Cancer Observatory concluded that it varies from 2-30 cases per 1,00,000 people worldwide. The highest incidence rate has been reported to be in South and Central Asia. In India, OSCC has become a public health problem due to its high incidence, accounting for 30% of all cancers [4]. The mortality rate of OSCC is also reported to be as high as 50% globally, with late diagnosis cited as an important reason behind the high mortality rate. While consumption of tobacco is the cause behind nearly 80% of all cases of OSCC, alcohol consumption [5] and exposure to the human papillomavirus (HPV) strains such as HPV-16 and HPV-18, are also identified as risk factors of OSCC in the oropharyngeal region [6].

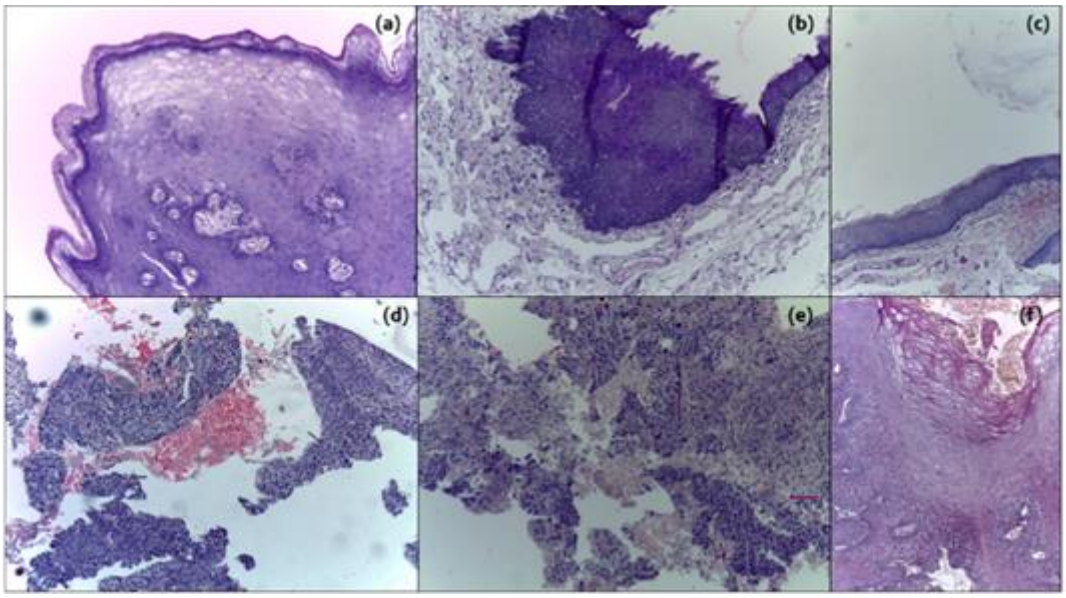

Figure 1 Illustrative examples from 'Normal' (a-c) & 'OSCC' (d-f)

The clinical implication of OSCC are highly dependent on the location and the stage of the cancer as early stages could be asymptomatic or pose as an ulcer or leukoplakic lesion. Patients with further stages report pain and bleeding in the oral cavity along with facial swelling and numbness. The diagnosis of involves initial clinical examination followed by medical imaging of

the region and biopsy, the latter of which is considered to be the gold standard. Here, a sample of the tissue is removed and used for histopathological examination.

The histological features of OSCC are identified by the presence of the malignant cells with varying degrees of differentiation and alterations in the architecture of the surrounding tissue. Histopathology is also useful for detecting the presence of biomarkers associated with OSCC, such as p53, Ki-67, and cyclin D1. These biomarkers are often overexpressed in OSCC and can be detected by immunohistochemical staining of tissue sections [7]. The presence of these biomarkers may provide prognostic information and help guide treatment decisions, digital pathology and image analysis have shown promise in improving the accuracy and efficiency of OSCC diagnosis. Digital pathology involves the use of digital images of tissue specimens, which can be viewed and analysed using specialized software [8]. Image analysis techniques such as computer-aided diagnosis (CAD) can be used to automatically identify and quantify histological features of OSCC, such as cell morphology, nuclear size, and mitotic activity. These techniques have the potential to improve diagnostic accuracy and reduce inter-observer variability.

The usage of deep convolutional neural networks has shown promise in improving the accuracy and efficiency of oral squamous cell carcinoma (OSCC) using histopathology images. These approaches involve the use of convolutional neural networks (CNNs) to automatically learn and extract meaningful features from histopathological images. This work builds on this domain by using a publicly available histopathology dataset to develop a deep learning-based classifier using transfer learning. InceptionV3, the pre-trained convolutional neural network selected when trained with the pre-processed dataset yields a reliable accuracy of 96.89% and F1-Score for the diseased class of 0.9569.

II. Methodology

Detailed in this section is the pre-experimental and experimental procedure including details about the dataset used, the pre-processing techniques applied and the hyperparameters used during the training of the convolutional neural networks.

A. Dataset

The dataset used in this work is a publicly available binary class dataset on Kaggle [9]. The dataset has curated using biopsies that are stained and then photographed using a microscopic lens. The two classes of the dataset 'Normal' and 'OSCC' have 2494 and 2698 images respectively.

The images consist of histopathology images with magnification factors of 100x and 400x. The images have significant variations amongst themselves, with varied resolutions and aspect ratios. Using pre-processing techniques discussed in Section II.B, the non-uniform images have been pre-processed to serve as the input for the convolutional neural network discussed in Section II.C.

B. Pre-Processing

Due to the resolution and aspect ratio inconsistencies in the dataset used in the training and the validation of the deep learning models in this work, image pre-processing played a big hand in getting usable results from the dataset and improving the robustness of the training. Four pre-processing methods were explored in this work as represented in Image 2: Reinhard's method, contrast enhancement, unsharp masking and resizing.

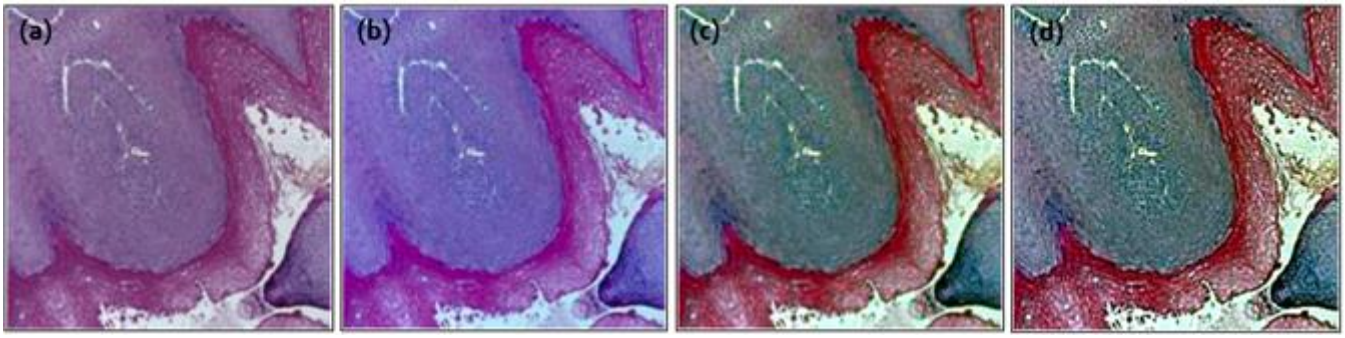

Figure 2 Image undergoing (a) Resizing (b) Colour Normalization (c) Contrast Enhancement (d) Unsharp Masking

Reinhard's Method is a colour normalization technique commonly used for histopathology images [10]. Here, the colour distribution of the image is mapped to that of a reference image. When performed on the dataset, this method enables the colours of the histopathology images to be more consistent across the dataset. The colour distribution of the dataset image are fundamentally aligned using a non-linear transformation to a target image which is computed using a histogram matching approach that minimize the difference between two distributions. The colour distributions of the dataset and the reference images are calculated approximately by using Gaussian distributions and the non-linear transformation is represented by global colour transfer function. The normalization of the colour distribution of the image is computed by the standard deviation and the mean deviation in the reference and dataset for each colour channel: red, blue and green.

The global transfer function that is calculated from this is represented in Equation (1). This then maps the pixel values in the input image to the new values from the generated colour distribution.

$$f(x) = \sigma_r / \sigma_g * (x - \mu_t) + \mu_r \qquad (1)$$

In equation (1) x represents the pixel values in the input image and μ_t and σ_g are the mean and standard deviation of the target image, μ_r and σ_r are the mean and standard deviation of the reference image and f(x) is the corresponding pixel value in the transformed image. After mapping the standard and mean deviation of the colours using the defined transfer function, the colour distribution is more consistent across the dataset and serves as a better dataset for training and validation of the deep learning model. Several studies have employed this pre-processing technique to normalize the colour distribution across the dataset for the histopathology images [11] [12].

A two-fold contrast enhancement technique has been used in this this work as contrast enhancement techniques have proven to be an effective histopathology image pre-processing technique as shown in in the works in [13] [14]. The sharpening is performed by mapping the original pixel intensities to a new range of values ranging between 0 and 1, after which the limits of the pixel intensity range is computed before stretching. A 5x5 Gaussian filter is created and applied to the image for smoothing the image and reducing the noise in it. Finally, unsharp masking is performed on the image which is done by subtracting a blurred version of the image from the original image and then computing and adding scaled back version of the original image. The final image has sharpened edges with enhanced contrast. Due to the inconsistency in the resolution and aspect ratios of the images, the entire dataset was resized to 224x224 across the three channels. This also resulted in a uniform 1:1 aspect ratio for all images for training and validation.

C. Deep Learning Approach

While the dataset used in this study has 5192 images, which is large enough to train a fully custom convolutional neural network, transfer learning can be used to build on the pre-trained weights of the neural networks for better model accuracy. An evolution of the Inception family of pre-trained convolutional neural networks, InceptionV3 is the third generation of pre-trained CNNs from Google Inc. introduced in 2015 [15]. The version of InceptionV3 used in this study has been trained on the ImageNet dataset, a dataset having over 12 lakh training images across 1000 classes.

The fundamental unit of InceptionV3 are Inception Modules. These modules depicted in Figure 3, are multiple parallelly arranged convolutional layers having varying filter sizes that allow for the learning global and local features of an image. In this network, convolution layers with filter sizes 1x1 and 3x3 are used.

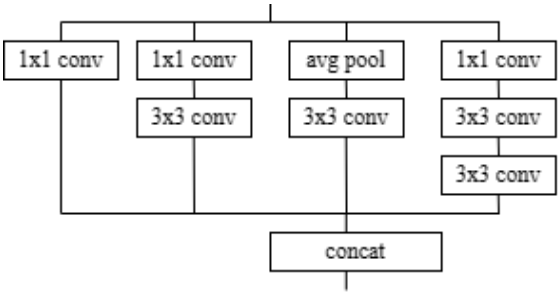

Figure 3 Inception Module in InceptionV3

InceptionV3 adds to the pre-existing Inception Modules with auxiliary classifiers that are placed in intermediate layers of the network that learn features more discriminative to the classification training. As shown in Figure 4, it comprises of pooling, convolutional, fully connected and SoftMax layers, the auxiliary classifiers help solve the vanishing gradient problem that arises during the training of convolutional neural networks.

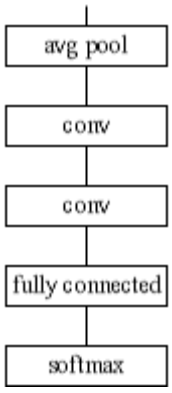

Figure 4 Auxiliary Classifier in InceptionV3

This network has been widely used in object detection, image segmentation and classification training and validation experiments since its launch. Using InceptionV3 as a pre-trained model for transfer learning has been shown to be effective in various computer vision tasks. The study conducted in [16] used transfer learning with InceptionV3 to classify breast cancer histology images and achieved a classification accuracy of 92%.

The optimization technique employed on the InceptionV3 model is the Stochastic Gradient Descent with Moment (SGDM) solver. This optimizer builds on the standard Stochastic gradient Descent (SGD) optimizer that updates parameters in small batches using the gradient of the cost function of each parameter till it is minimized to a satisfactory level. SGDM adds a momentum term that solved the slow convergence when gradients are noisy, or cost function used has multiple local minima. The addition of this momentum term serves as a moving average of the gradients to dampen the update process oscillations that smoothens it and accelerate convergence by maintaining consistent direction to the minimum of the cost function [17].

D. Experimental Setup

The pre-processing of the images and the training and the validation of the InceptionV3 based network have all been performed on MathWorks MATLAB 2022b with the Computer Vision Toolbox and Deep Learning Toolbox installed. The Image Batch Processor app has been used to perform the pre-processing on the images and Experiment Manager has been used to conduct the training and validation trials. The execution environment for the image pre-processing tasks was the single CPU while the execution environment was set to the single GPU utilizing Nvidia CUDA.

Table 1 Parameters of top performing trial

Parameter	***Value***
Network	Inceptionv3
Solver	SGDM
Epochs	5
Batch Size	32
Learn Rate	0.001
Execution Environment	Single GPU

After careful trial and error, the experimental hyperparameters used for the top performing trial have been detailed in Table 1. The CUDA enabled GPU aided in the acceleration of the training and the validation of the networks while the Stochastic Gradient Descent with Moment solver was selected due to its prevalence and reliability in medical image classification works. The batch size of 32 helped leverage the 4GB VRAM available in the GPU and the learn rate 0.001 and epoch size 3 enable the network to achieve best results.

III. RESULTS

In this section, the results of the top performing trial, the parameters of which have been represented in Table 2, will be discussed along with calculated performance evaluation metrics.

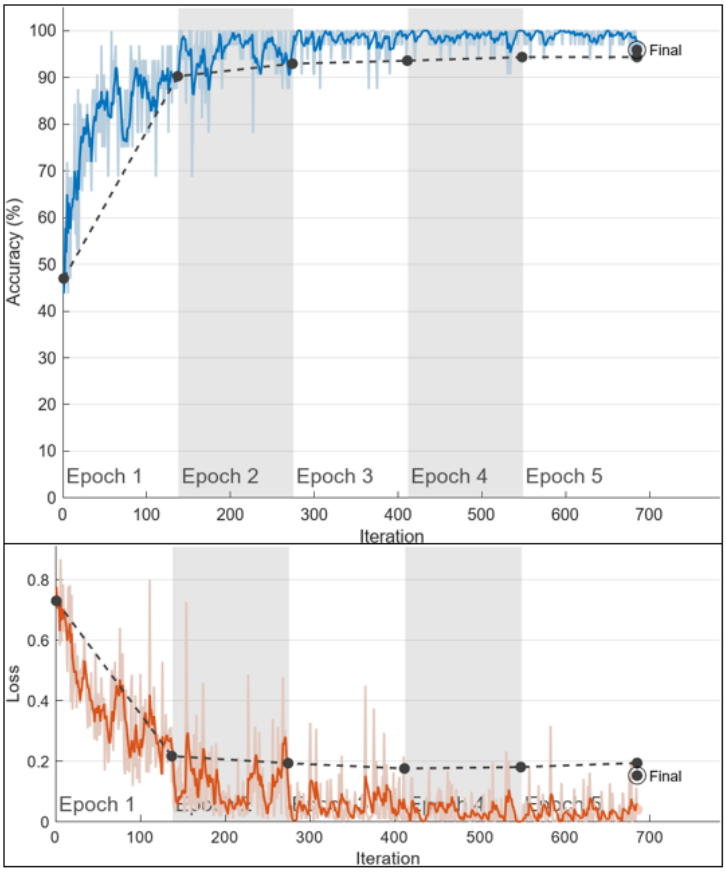

Figure 5 Accuracy & Loss Plots

A. *Performance Evaluation Metrics*

For the evaluation of the binary classification experiment, the several metrics can be calculated using the 2x2 confusion matrix generated for the validation portion, alongside the accuracy and loss curves as represented in Figure 5, of the neural networks that represents the true positives, true negatives, false positives, and false negatives. The true class in this case is class 'OSCC' while class 'Normal' represents the false class. The accuracy of a binary classifier represents the ratio of the correctly classified validation data to the entire validation data. The precision of a classifier represents the ratio of the true positives to the sum of all predicted positive samples in the validation data. The recall represents the ratio of the true positives all actual true values of the validation data. Using the calculated recall and precision, an F1-Score can be calculated that more accurately evaluates the performance of each class of the classifier.

B. *Experimental Results*

The experimental results obtained in the transfer learning experiment have been represented in Table 2. Out of the best performing trials, the top performing InceptionV3 that ran for three epochs netted the highest accuracy of 0.9589 or 95.89% while the validation loss was low at 0.1534. The InceptionV3 trial that ran for only two epochs netted a lower accuracy of just 0.9023 or 90.23% while the validation loss was slightly higher at 0.2755. Interestingly, the training accuracy was reported to be identical across the two trials at 0.9687 or 96.87% which could indicate scope for further optimization of the dataset or training hyperparameters.

Table 2 Reported Training & Validation Performance

	Training		**Validation**		***Duration***
Epochs	**Accuracy**	**Loss**	**Accuracy**	**Loss**	***(seconds)***
5	***0.9687***	***0.0407***	***0.9589***	***0.1534***	*1915*
2	0.9687	0.0669	0.9023	0.2755	***1178***

C. *Calculated Metrics*

For the evaluation of the models as described in Section 3.1, the values from the confusion matrix have been represented in Table 3. The 5% gap between the two trials can be confirmed with the far more misclassified class 'OSCC' validation samples. This can be further explored in Table 4.

Table 3 Values from the Confusion Matrices

Epochs	***True Positive***	***True Negative***	***False Positive***	***False Negative***
5	***355***	***392***	***19***	***13***
2	370	341	4	64

Although the number of correctly classified positive class samples is higher in the trial conducted with only two epochs, the far greater number of false negatives impacts the sensitivity and the F1-Score of the classifier. This indicates that that the robustness of the trial that ran for five epochs is still better than that of the trial that ran for two epochs due to the higher F1-Score.

Table 4 Calculated Performance Metrics

Epochs	***Sensitivity***	***Specificity***	***Precision***	***F1 Score***
5	***0.9647***	*0.9539*	*0.9492*	***0.9569***
2	0.8525	**0.9884**	**0.9893**	0.9158

A. *Explaining Model Predictions*

The explainable AI method LIME have been used to generate heatmaps that explain the reasoning behind a model's predictions. LIME (Local Interpretable Model-agnostic Explanations) is a model explain-ability method that generates heatmaps to explain the predictions of machine learning models. LIME generates a heatmap that shows the regions of an image that were most influential in a model's prediction [18]. The heatmaps and segmentations performed by LIME have been depicted in Figure 6.

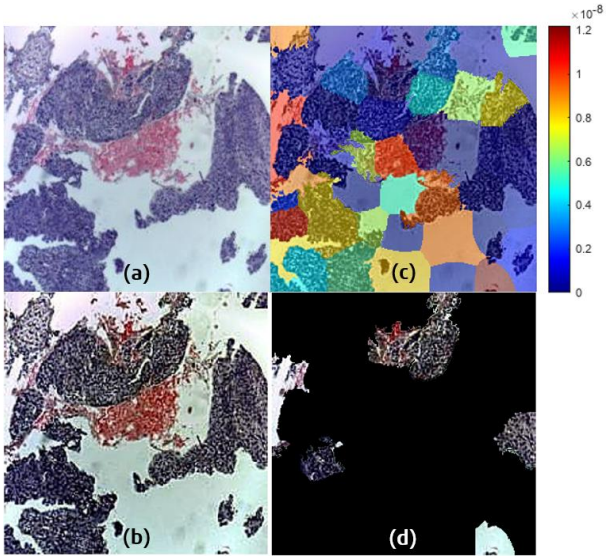

Figure 6 Explainable AI generated heatmaps and segmentation. (a) Original Image (b) Image after processing (c) LIME based super pixel heatmap distribution of important features (d) Top 7 features segmented from LIME heatmap.

From the final segment of the top seven features used to make predictions in Fig. 4(d), it can be observed that out of the seven superpixels displayed, all but two have used correct parameters for making the prediction. Further optimization can be done to minimize innacurate predictions and improve the overall performance of the classifier.

IV. Conclusion & Future Scope

The use of the InceptionV3 based classifier on pre-processed OSCC histopathology images resulted in an impressive accuracy of 95.69%. The pre-processing of images helped in enhancing the image quality and reducing the effect of noise, leading to improved classification results and being able to achieve a result of 100% in the training accuracy. The use of deep learning techniques has shown promising results in the field of medical image analysis, especially in the early detection and diagnosis of diseases like oral squamous cell carcinoma. As the convolutional neural network used in as the basis of the model is performant while also being efficient, it can be easily deployed on pre-existing hardware in a workflow pipeline as described in Figure 7.

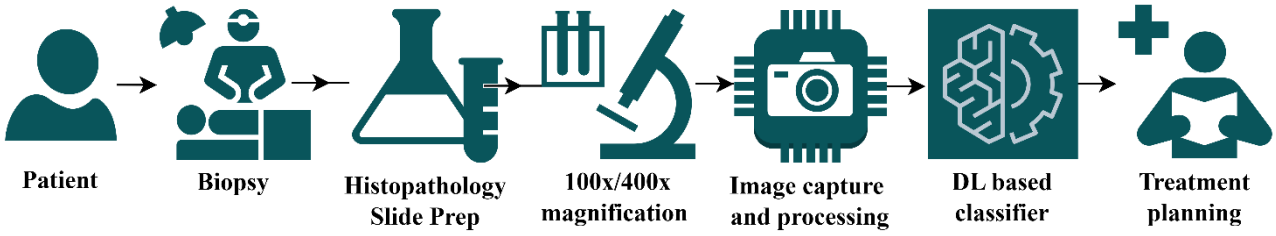

Figure 7 Ideal implementation pipeline for proposed model

The future scope of this research includes improving the performance of the classifier by using more advanced deep learning architectures or using meta learning and ensemble learning along with more robust pre-processing. Additionally, the development of computer-aided diagnosis systems can aid pathologists in detecting and diagnosing diseases more accurately and efficiently. Furthermore, the use of multi-modal imaging techniques, such as combining histopathology images with radiological images, can enhance the accuracy of diagnosis and reduce the subjectivity in the interpretation of images.

References

[1] Neville, B. W., & Day, T. A. (2002). Oral cancer and precancerous lesions. CA: a cancer journal for clinicians, 52(4), 195-215.

[2] Oral Health. (n.d.). Retrieved March 2, 2023, from https://www.who.int/news-room/fact-sheets/detail/oral-health

[3] Oral Cavity & oropharyngeal cancer key statistics 2021. (n.d.). Retrieved March 1, 2023, from https://www.cancer.org/cancer/oral-cavity-and-oropharyngeal-cancer/about/key-statistics.html

[4] Kuriakose, M., Sankaranarayanan, M., Nair, M. K., Cherian, T., Sugar, A. W., Scully, C., & Prime, S. S. (1992). Comparison of oral squamous cell carcinoma in younger and older patients in India. European Journal of Cancer Part B: Oral Oncology, 28(2), 113-120.

[5] Blot, W. J., McLaughlin, J. K., Winn, D. M., Austin, D. F., Greenberg, R. S., Preston-Martin, S., ... & Fraumeni Jr, J. F. (1988). Smoking and drinking in relation to oral and pharyngeal cancer. Cancer research, 48(11), 3282-3287.

[6] Secretan, B., Straif, K., Baan, R., Grosse, Y., El Ghissassi, F., Bouvard, V., ... & Cogliano, V. (2009). A review of human carcinogens—Part E: tobacco, areca nut, alcohol, coal smoke, and salted fish. The lancet oncology, 10(11), 1033-1034.

[7] Ahmed, H. G. (2013). Aetiology of oral cancer in the Sudan. Journal of oral & maxillofacial research, 4(2).

[8] Pantanowitz, L., Sinard, J. H., Henricks, W. H., Fatheree, L. A., Carter, A. B., Contis, L., ... & Parwani, A. V. (2013). Validating whole slide imaging for diagnostic purposes in pathology: guideline from the College of American Pathologists Pathology and Laboratory Quality Center. Archives of Pathology and Laboratory Medicine, 137(12), 1710-1722.

[9] Kebede, A. (2021, July 21). Histopathologic oral cancer detection using CNNS. Retrieved January 6, 2023, from https://www.kaggle.com/datasets/ashenafifasilkebede/dataset

[10] Vahadane, A., Peng, T., Albarqouni, S., Baust, M., Steiger, K., Schlitter, A. M., ... & Navab, N. (2015, April). Structure-preserved color normalization for histological images. In 2015 IEEE 12th international symposium on biomedical imaging (ISBI) (pp. 1012-1015). IEEE.

[11] Roy, S., kumar Jain, A., Lal, S., & Kini, J. (2018). A study about color normalization methods for histopathology images. Micron, 114, 42-61.

[12] Steiner, D. F., MacDonald, R., Liu, Y., Truszkowski, P., Hipp, J. D., Gammage, C., ... & Stumpe, M. C. (2018). Impact of deep learning assistance on the histopathologic review of lymph nodes for metastatic breast cancer. The American journal of surgical pathology, 42(12), 1636.

[13] Guzmán-Cabrera, R., Guzmán-Sepúlveda, J. R., Torres-Cisneros, M., May-Arrioja, D. A., Ruiz-Pinales, J., Ibarra-Manzano, O. G., ... & Parada, A. G. (2013). Digital image processing technique for breast cancer detection. International Journal of Thermophysics, 34, 1519-1531.

[14] Wang, P., Hu, X., Li, Y., Liu, Q., & Zhu, X. (2016). Automatic cell nuclei segmentation and classification of breast cancer histopathology images. Signal Processing, 122, 1-13.

[15] Szegedy, C., Vanhoucke, V., Ioffe, S., Shlens, J., & Wojna, Z. (2016). Rethinking the inception architecture for computer vision. In Proceedings of the IEEE conference on computer vision and pattern recognition (pp. 2818-2826).

[16] Litjens, G., Kooi, T., Bejnordi, B. E., Setio, A. A. A., Ciompi, F., Ghafoorian, M., ... & Sánchez, C. I. (2017). A survey on deep learning in medical image analysis. Medical image analysis, 42, 60-88.

[17] Qian, N. (1999). On the momentum term in gradient descent learning algorithms. Neural networks, 12(1), 145-151.

[18] Ribeiro, M. T., Singh, S., & Guestrin, C. (2016). Model-agnostic interpretability of machine learning. arXiv preprint arXiv:1606.05386.

Binary Detection of Acute Lymphocytic Leukemia Using Segmented Blood Smear Images Using Deep Learning Models

Nitla Gokulkrishnan
Department of Biomedical Engineering
Manipal Institute of Technology
Manipal Academy of Higher Education
Manipal, India
nitilagokulkrishnan@outlook.com

Lavanya Dalmia
Department of Biomedical Engineering
Manipal Institute of Technology
Manipal Academy of Higher Education
Manipal, India
lavanya1.mitmpl2022@learner.manipal.edu

Tushar Nayak
Department of Biomedical Engineering
Manipal Institute of Technology
Manipal Academy of Higher Education
Manipal, India
https://orcid.org/0000-0002-4328-7983

Reva Laghate
Department of Biomedical Engineering
Manipal Institute of Technology
Manipal Academy of Higher Education
Manipal, India
reva1.mitmpl2022@learner.manipal.edu

Niranjana Sampathila*
Department of Biomedical Engineering
Manipal Institute of Technology
Manipal Academy of Higher Education
Manipal, India
https://orcid.org/0000-0002-3345-360X

***Abstract*— Leukemia is a type of blood cancer that can be difficult to diagnose and treat, and early detection is crucial for improving patient outcomes. In recent years, deep learning techniques have shown great potential in improving the accuracy and efficiency of cancer detection. In this paper, we present a novel approach to detecting leukemia using deep learning. Specifically, we use a convolutional neural network (CNN) to analyze blood cell images and classify them as either leukemia or non-leukemia cells. The model chosen for this study was ResNet50. The model was trained on a large dataset of blood smear images with varying hyperparameters, achieving an accuracy over 92%. Overall, our study highlights the potential of deep learning in revolutionizing the diagnosis and treatment of leukemia. By leveraging the power of deep learning, we can improve the accuracy and efficiency of leukemia detection, leading to earlier detection and better patient outcomes at reduced healthcare costs.**

Keywords*— *Blood Cancer, Blood Smear, Deep Learning, Acute Lymphocytic Leukemia, Digital Pathology

I. INTRODUCTION

There are several technological revolutions in the healthcare industry that aim at a cancer-free society. Technologies like nanomedicine, targeted therapy, gene therapy, thermal ablation, magnetic hyperthermia and extra cellular vehicles can be used for improved cancer diagnosis and treatment [1].Blood cancer is a condition that serves as a major challenge to it. Leukemia along with lymphoma, myeloma, myelodysplastic syndrome (MDS), myeloproliferative neoplasms (MPS) are types of blood cancer that together constitute nearly six percent of all global cancer cases [2].

Leukemia is associated with uncontrolled production (abnormal cloning) of hematopoietic stem cells in the bone-marrow. It is generally classified depending on its effects on the myeloid (granulocytes or monocytes) line of blood cells or the lymphoid (T-cells, B-cells, NK cells) line of blood cells and further classified into acute or chronic. These are namely Acute Lymphoblastic Leukemia (ALL), Acute Myeloid Leukemia (AML), Chronic Lymphocytic Leukemia (CLL) and Chronic Myeloid Leukemia (CML) [3] ALL deals with the release of immature lymphocytes (blast cells) in the bloodstream which results in a drop in the RBC and platelet counts. These blast cells are inefficient in fighting bacteria and viruses.

Presently 2.5% of all blood cancer cases are leukemia [4] amongst which 30% to 35% of the cases are of acute lymphoblastic leukemia (ALL). In 2017, the global incidence of ALL was 1.04 cases per 100,000 people, while the global mortality was 0.72 deaths per 100,000 cases [5]. Between 2013-2017 highest mortality rates for leukemia were reported in Venezuela, Ecuador, Nicaragua, Mexico, and Peru in the Latin America and Caribbean countries (LAC) [6]. In 2022 about 6,660 people of all ages were diagnosed with ALL in the US and estimated death count was 1,560 deaths [7]. More than 10,000 new cases of childhood ALL are expected in India annually [8].

The exact aetiology of Acute Lymphocytic Leukemia is unknown although exposure to benzene, ionizing radiation, chemotherapy and radiotherapy are high risk factors [9]. Genetic factors like hypodiploidy, Philadelphia (Ph) chromosome, mixed lineage leukemia (MLL)/11q23 rearrangement, multiple chromosomal aberrations, persistence of minimal residual disease (MRD) are also suggested to play a role, [10] but ALL is not to be considered as a familial disease. Symptoms include pale skin, easy bruising/bleeding, weakness, weight loss, or difficulty breathing [11]. Acute lymphocytic leukemia is recognized to be cured if the affected is in total remission for 10 years. While children show survival rates above 90%, in adults these numbers stand at 35-45% for the same treatments. However, the cured are susceptible to complications due to treatment [12].

It is a rare disease yet the most common type of leukemia that affects children. It prevails commonly in children with an incident rate four times that of an adult. If diagnosed at an early stage, leukemia can be treated. To aid this early detection, in this work we propose a deep learning-based approach for the detection of ALL using the pretrained convolutional neural network,

ResNet50. Our approach is based on the analysis of blood smear images, obtained from a publicly available dataset. We have used the ALL Challenge dataset of ISBI 2019 (C-NMC 2019) [13] which has been segmented and pre-processed to isolate the relevant features. We demonstrate that out approach achieves an accuracy of 92%, which is comparable with the traditional visual inspection methods. Our results demonstrate the potential of deep learning in revolutionizing the field of leukemia detection, leading to earlier and more accurate diagnosis, at reduced healthcare costs.

II. Methodology

This section details the dataset used for transfer learning, the deep learning architectures used and the experimental setup.

A. Dataset

This study makes use of the C-NMC Acute Lymphocytic Leukemia Dataset. This dataset was used in the C-NMC 2019 Challenge in which participants competed to develop robust and accurate classifiers for hematopoietic cells in leukemia patients. The 450x450 resolution images in this dataset have been acquired using a Leica DM LB microscope and 100x oil immersion objective lens. After acquisition, the images have also been pre-processed for artefact removal, normalization, and centring [13]. Samples from the two classes of the dataset have been detailed in Fig. 1.

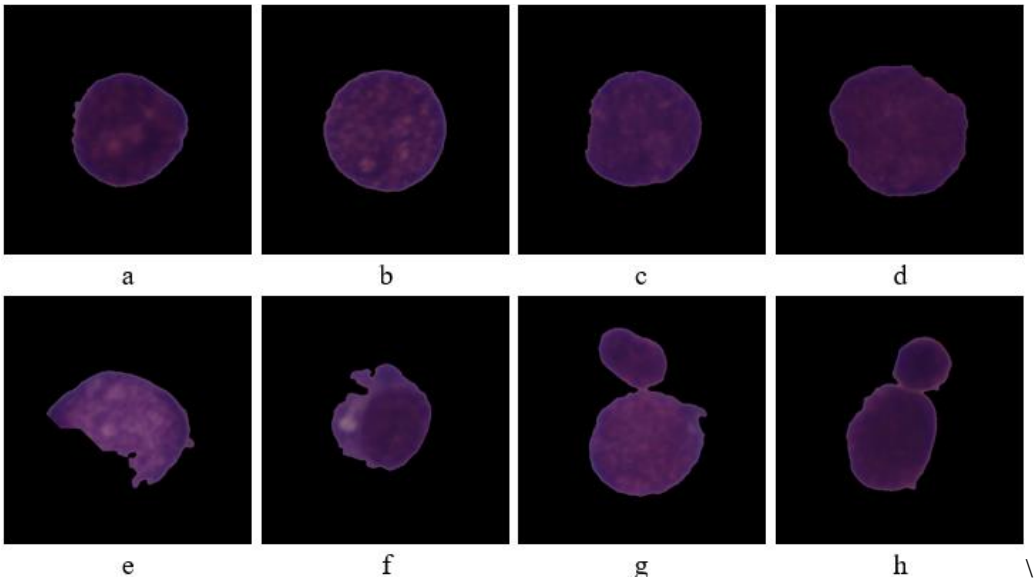

Fig. 1. a-d belong to the normal class whereas e-h represent leukemic cells.

As this work serves as a precursor to a future study to be conducted with a more complex dataset, the entire dataset has not been used. Here, only a small set of the images have been used for the transfer learning experiment trials. The full dataset contains 10661 images in which class 'ALL' contains 7272 images and class 'HEM' contains 3389. The approximate 2:1 ratio of the entire dataset has been replicated in the subset of data used in this study. The 1867 images of this dataset subset are divided into 1219 images in class 'ALL' and 648 images in class 'HEM'.

B. Deep Learning Architectures

The deep convolutional neural network used in the training and validation of the transfer learning experiment in this study is ResNet50. Introduced in [14] in the year 2015 by researchers at Microsoft Inc, this convolutional neural network makes use of residual blocks to solve the vanishing gradient problem. These skip connections allow for information passage in the neural network without loss as the network is built deeper. Effectively, this solves the problem where gradients vanish due to the increasing depth of the neural networks. The benefit of this help with increasing the effective training accuracy of these ResNets. Due to their robustness, Residual Networks have been successfully employed in deep learning-based image classification, object detection and segmentation. In the field of medical informatics, ResNet50 has been used for a variety of tasks, including disease classification and segmentation.

For example, [15] used ResNet50 to classify breast lesions in mammograms with an accuracy of 87.2%. The authors of [16] used ResNet50 to classify pulmonary nodules in chest CT scans with an accuracy of 91.3%. ResNet50 has also been used for brain tumour segmentation [17] and diabetic retinopathy detection [18] with promising results.

C. Experimental Setup

The experiment was conducted using the Experiment Manager app, a part of the Deep Learning Toolbox, on MATLAB 2022b. The training environment was set to the single GPU, a Nvidia GTX 1650 (Laptop) with 4GB VRAM. Using the Deep Learning Toolbox, the pre-trained network ResNet50 was installed for training and validation on the given dataset. The Stochastic Gradient Decent (SGD) solver has been employed to train the ResNet model. The hyperparameters used during all the trials have been detailed in Table 1. Highlighted values in Table 1 are the hyperparameters of the top performing trial.

Table 1 Hyperparameters selected for training the models.

Hyperparameter	***Value***
Epochs	*2 5* ***10***
Batch Size	***128*** *256*
Learn Rate	***0.001*** *0.0001*
Networks	***ResNet50***

Other hyerparameters selected for the trials include the stochastic gradient decent with moment solver for all trials and the validation frequency as once every epoch.

III. Results and Discussions

This section details the metrics used to evaluate the performance of the neural network for the different hyperparameters, the results obtained, the calculated performance and lastly compares our work with existing work in the domain.

A. Preformance Evaluation Metrics

To calculate the performance of the deep convolutional neural network-based classifiers, the accuracies for the training and validation of the different trials have been considered. Along with the accuracy, three other parameters: sensitivity, recall and f1 score have also been calculated for class 'ALL' to better shed light on the performance of the model. These parameters have been calculated using the confusion matrix generated after the validation of each trial. A sample confusion matrix has been represented in Fig.2.

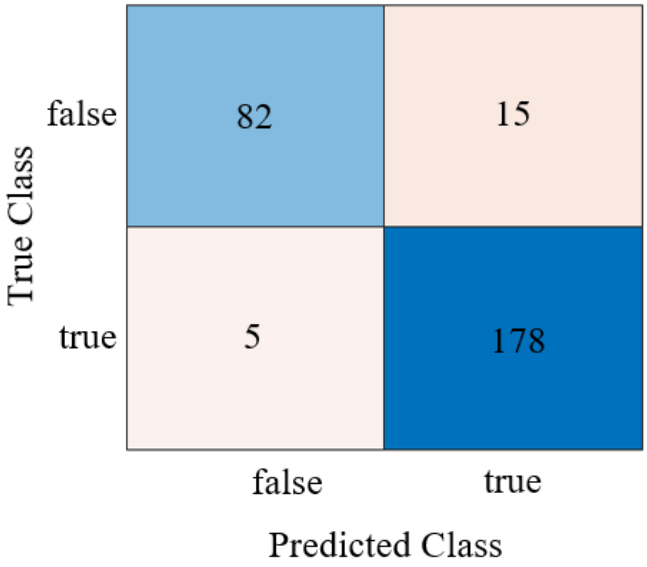

Fig. 2 Confusion Matrix

The accuracy of a classifier measures the proportion of the correct predictions made by it to all predictions made. The sensitivity is the true positive rate of the classifier, and it measures the proportions of all correctly classified positive samples. The specificity is the true negative rate of the classifier, and it measures the proportion of all correctly classified negative samples. The precision is the proportion of true positive predictions made by a classifier to all positive predictions, true and false. The F1 Score of a network is the harmonic mean of the precision and recall that provides a unified performance metric for each class when the dataset is unequally distributed across the classes.

B. Experimental Results

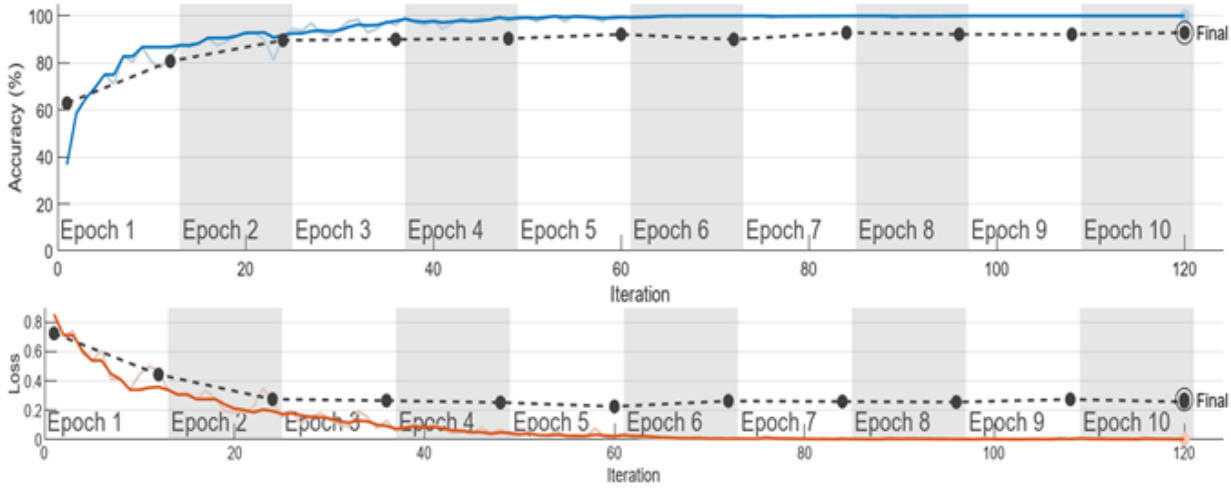

Fig. 3 Accuracy and Loss curves

The accuracies and losses of training and validation along with the time elapsed for each trial for the highest performing iterations of the chosen model have been detailed in Table 2. It was observed that the model performed best with a learn rate set to 0.001, for batch size 128. Sample accuracy and loss curves have been illustrated in Fig. 3.

Table 2 Training results for the models for varied hyperparameters

Trial Number	Epochs	Time	Training		Validation	
			Accuracy	Loss	Accuracy	Loss
Trial 1	*2*	*328sec*	*0.91*	*0.2596*	*0.9071*	*0.2818*
Trial 2	*5*	*673sec*	*1*	*0.027*	*0.9107*	*0.2537*
Trial 3	***10***	***1321sec***	***1***	***0.0013***	***0.9286***	***0.2740***

The network achieved an accuracy of 92.86% when trained for 10 epochs with batch size set to 128 with 0,001 as the learn rate. It has also been shown that the iterations elapsed in relatively short durations of time, thus illustrating how deep learning based models speed up the process of disease diagnosis. The values obtained from the confusion matrix of the best trial are detailed in Table 3.

Table 3 Values obtained from the validation confusion matrices generated.

Trial Number	Accuracy	True Positive	True Negative	False Positive	False Negative
Trial 3	*0.9286*	*178*	*82*	*15*	*5*

C. Calculated Performance Parameters

The performance of the top performing trials of the ResNet50 model can be evaluated by using parameters: accuracy and the sensitivity, precision, recall and F1-score for class ‘ALL’ as discussed in Section A. Table 4 illustrates the performance of the best performing trial. The model achieved an accuracy of 92.86% and an F1-score of 0.9468.

Table 4 Evaluation Matrices of the highest performing trial

Trial Number	Accuracy	Sensitivity	Specificity	Precision	F1 Score
Trial 3	*0.9286*	*0.9223*	*0.9425*	*0.9727*	*0.9468*

D. Comparison with existing work

Acute lymphoblastic leukemia (ALL) is a type of cancer that affects the blood and bone marrow. Early detection and accurate diagnosis are crucial for successful treatment. Deep learning, a type of artificial intelligence, has been explored as a potential tool for detecting ALL from blood smear images. C-NMC Acute Lymphoblastic Leukemia dataset has been used widely to train deep learning models since it is publicly available.

In [19] the authors have performed a four-fold augmentation on the image dataset before training it on a custom convolutional neural network architecture to classify between blast cells and healthy ones. They achieved an accuracy of 0.95. In the study [20] the images in the dataset have been normalized and undergone contrast enhancement. The model chosen was ResNet18 and yelled F1-score of 0.87. In the study [21] the authors have normalized and centre cropped the images before using them to train a deep learning model built by stacking InceptionV3, DenseNet121 and InceptionResNetV2 to achieve a weighted F1-score of 0.86. In [22] the authors have performed Contrast limited adaptive histogram equalization (CLAHE) on the dataset before training it on a Modified VGG-16 to achieve an F1-score of 0.91.

Our proposed work uses a modified pretrained residual network ResNet50 with varying hyperparameters to optimize the model generating an F1-score above 0.94, classifying Leukemic blast cells from normal white blood cells with an accuracy of 92.8%.

IV. Conclusion and Future Scope

In conclusion, our study demonstrates the potential of deep learning for improving the accuracy and efficiency of disease detection. In this paper we have used the convolutional neural network ResNet50 to analyse blood smear images, to detect Acute lymphoblastic leukemia (ALL). Our results indicate that this approach achieved an accuracy of 92.8%, demonstrating its effectiveness in diagnosing leukemia with high accuracy in a relatively short period of time. Deep learning techniques have been shown to outperform traditional methods of leukemia detection and have the potential to be integrated into clinical practice, providing doctors with a reliable tool for diagnosing leukemia. The high accuracies achieved in a shortened amount of time, lead to early diagnosis and better patient outcomes. Furthermore, this method has a potential to reduce healthcare costs by eliminating the need for invasive and time-consuming diagnostic procedures.

Future research in the field of leukemia detection using deep learning has numerous avenues for exploration. One possible direction is the development of multi-modal deep learning models that can analyse various types of leukemia data, including blood cell images, bone marrow images, and flow cytometry data. Such models can provide a comprehensive and accurate diagnosis by combining the strengths of different imaging techniques. Another potential area for future research is the integration of deep learning models with electronic health records (EHRs) to provide personalized treatment recommendations and real-time decision support for clinicians. These models can utilize patient data, including imaging data, genomic data, and clinical data, to predict treatment outcomes and patient prognosis. Additionally, integrating deep learning models with EHRs can enable the efficient analysis of vast amounts of data to improve patient outcomes and reduce healthcare costs.

In conclusion, further research in deep learning-based approaches for leukemia detection can lead to improved accuracy and efficiency of diagnosis, which can ultimately lead to better patient outcomes. With the increasing availability of healthcare data and advancements in deep learning techniques, the potential for further development in this field is significant.

References

[1] Pucci, C., Martinelli, C., & Ciofani, G. (2019). Innovative approaches for cancer treatment: Current perspectives and new challenges. Ecancermedicalscience, 13.

[2] What is blood cancer? (n.d.). Retrieved March 2, 2023, from https://bloodcancer.org.uk/understanding-blood-cancer/what-is-blood-cancer/

[3] Chen, J., Huang, C., Zhu, Y., Dong, L., Cao, W., Sun, L., ... & Wang, C. (2015). Identification of similarities and differences between myeloid and lymphoid acute leukemias using a gene-gene interaction network. Pathology-Research And Practice, 211(10), 789-796.

[4] Worldwide cancer data: World cancer research fund international. (2022, April 14). Retrieved March 2, 2023, from https://www.wcrf.org/cancer-trends/worldwide-cancer-data/

[5] Fernandes, M. R., Souza Vinagre, L. W. M., Rodrigues, J. C. G., Wanderley, A. V., Fernandes, S. M., Gellen, L. P. A., ... & Santos, N. P. C. D. (2022). Correlation of Genetic Variants and the Incidence, Prevalence and Mortality Rates of Acute Lymphoblastic Leukemia. Journal of Personalized Medicine, 12(3), 370.

[6] Torres-Roman, J. S., Valcarcel, B., Guerra-Canchari, P., Santos, C. A. D., Barbosa, I. R., La Vecchia, C., ... & de Souza, D. L. B. (2020). Leukemia mortality in children from Latin America: trends and predictions to 2030. BMC pediatrics, 20(1), 1-9.

[7] Leukemia - acute lymphocytic - all - statistics. (2022, April 14). Retrieved March 2, 2023, from https://www.cancer.net/cancer-types/leukemia-acute-lymphocytic-all/statistics#:~:text=The%205%2Dyear%20survival%20rate%20for%20people%20age%2020%20and,disease%20and%20a%20person's%20age

[8] Kulkarni, K. P., Arora, R. S., & Marwaha, R. K. (2011). Survival outcome of childhood acute lymphoblastic leukemia in India: a resource-limited perspective of more than 40 years. Journal of pediatric hematology/oncology, 33(6), 475-479.

[9] Puckett, Y., & Chan, O. (2022). Acute lymphocytic leukemia. In StatPearls [Internet]. StatPearls Publishing.Worldwide cancer data: World cancer research fund international. (2022, April 14). Retrieved March 2, 2023, from https://www.wcrf.org/cancer-trends/worldwide-cancer-data/

[10] Papadantonakis, N., & Advani, A. S. (2016). Recent advances and novel treatment paradigms in acute lymphocytic leukemia. Therapeutic advances in hematology, 7(5), 252-269.

[11] (n.d.). Retrieved March 14, 2023, from https://www.nhs.uk/conditions/acute-lymphoblastic-leukaemia/

[12] Rafei, H., Kantarjian, H. M., & Jabbour, E. J. (2019). Recent advances in the treatment of acute lymphoblastic leukemia. Leukemia & lymphoma, 60(11), 2606-2621.

[13] C-NMC 2019 Challenge. (n.d.). Dataset. Retrieved February 26, 2023, from https://www.c-nmc.org/dataset

[14] He, Kaiming, et al. "Deep residual learning for image recognition." Proceedings of the IEEE conference on computer vision and pattern recognition. 2016.

[15] Wang, X., Liang, G., Zhang, Y., Blanton, H., Bessinger, Z., & Jacobs, N. (2020). Inconsistent performance of deep learning models on mammogram classification. Journal of the American College of Radiology, 17(6), 796-803.

[16] Wang, X., Mao, K., Wang, L., Yang, P., Lu, D., & He, P. (2019). An appraisal of lung nodules automatic classification algorithms for CT images. Sensors, 19(1), 194.

[17] Pawar, K., Chen, Z., Jon Shah, N., & Egan, G. F. (2020). An ensemble of 2D convolutional neural network for 3D brain tumor segmentation. In Brainlesion: Glioma, Multiple Sclerosis, Stroke and Traumatic Brain Injuries: 5th International Workshop, BrainLes 2019, Held in Conjunction with MICCAI 2019, Shenzhen, China, October 17, 2019, Revised Selected Papers, Part I 5 (pp. 359-367). Springer International Publishing.

[18] Porwal, P., Pachade, S., Kokare, M., Deshmukh, G., Son, J., Bae, W., ... & Meriaudeau, F. (2020). Idrid: Diabetic retinopathy–segmentation and grading challenge. Medical image analysis, 59, 101561.

[19] Sampathila, N., Chadaga, K., Goswami, N., Chadaga, R. P., Pandya, M., Prabhu, S., ... & Upadya, S. P. (2022, September). Customized Deep Learning Classifier for Detection of Acute Lymphoblastic Leukemia Using Blood Smear Images. In Healthcare (Vol. 10, No. 10, p. 1812). MDPI.

[20] Marzahl, C., Aubreville, M., Voigt, J., & Maier, A. (2019). Classification of leukemic b-lymphoblast cells from blood smear microscopic images with an attention-based deep learning method and advanced augmentation techniques. In ISBI 2019 C-NMC Challenge: Classification in Cancer Cell Imaging: Select Proceedings (pp. 13-22). Singapore: Springer Singapore.

[21] Ding, Yifan, Yujia Yang, and Yan Cui. "Deep learning for classifying of white blood cancer." ISBI 2019 C-NMC Challenge: Classification in Cancer Cell Imaging: Select Proceedings. Singapore: Springer Singapore, 2019. 33-41.]

[22] Honnalgere, A., & Nayak, G. (2019). Classification of normal versus malignant cells in B-ALL white blood cancer microscopic images. In ISBI 2019 C-NMC Challenge: Classification in Cancer Cell Imaging: Select Proceedings (pp. 1-12). Springer Singapore.

Development of Thermoreversible Hydrogel-based Bioink for 3D-Bioprinting and Tissue Engineering Applications

Dr. Anil Babu Katiki

Manipal Institute of Regenerative Medicine, MAHE, Bangalore, India

dr.anil.11248@gmail.com

*Dr. Manasa Nune

Manipal Institute of Regenerative Medicine, MAHE, Bangalore, India

manasa.nune@manipal.edu

***Abstract*— Biopolymers are used to formulate a hydrogel, which is then employed as the biomaterial ink to manufacture complicated tissue scaffolds that can more closely replicate clinical circumstances than 2D models. It requires a complex equilibrium between the factors that allow for complicated designs while not compromising the printed scaffold outcomes, consequently, each parameter's impact should be properly explored. The objective of this study was to establish and optimize the printing parameters necessary for effective 3D bioprinting. The Inkredible+, a commercial extrusion-based bioprinter with a pneumatic printhead, was utilized with varying print nozzle sizes. A composite hydrogel was created using different concentrations of Pluronic F-127 (PF127) and sodium alginate (SA) which demonstrated printability and cytocompatibility.**

Keywords— Pluronic, alginate, 3D Bioprinting, hydrogel, bioink, tissue engineering

I. INTRODUCTION

Three-dimensional (3D) bioprinting, which uses the precise placement of biomaterials and live cells to create sophisticated biological structures (tissues or organs), has led to the widespread application of advanced fabrication in tissue regeneration [1]. Bioinks are the principal elements used in 3D bioprinting. Bioinks are made up of a variety of biomaterials such as hydrogels, biomolecules, and living cells. The choices of biomaterials for bioinks are influenced by various aspects, including swelling, durability, printability, and biocompatibility [2]. There are 2 kinds of Bioprintable hydrogels: naturally produced hydrogels and synthetically derived hydrogels. Collagen, fibrin, hyaluronic acid, alginate, agarose, gelatin, and chitosan are the most commonly documented natural hydrogels, out of which collagen, fibrin, and gelatin contain innate signaling molecules for cell attachment [3]. Poly (ethylene glycol) (PEG), Pluronic, poly (vinyl alcohol) (PVA), and poly (caprolactone) are examples of synthetically generated hydrogels [4]. Owing to their outstanding biocompatibility and structural arrangements that are close to the ECM of native tissue, naturally generated hydrogels are the most often employed hydrogel compounds in tissue engineering applications [5]. Natural hydrogels, on the other hand, cannot sustain the printing design alone because of their poor tensile characteristics and quick biodegradability. As a result, composite bioinks built from natural and synthetic hydrogels have been created to address the shortcomings of bioprinting [6].

Pluronic F-127 (poloxamer 407) is a synthetic hydrogel composed of amphiphilic copolymers composed of polyethylene oxide and polypropylene oxide units. It is aqueous soluble and has a reversible gelation process [7]. Pluronic F-127 hydrogel also possesses advantageous qualities such as non-toxicity, cytocompatibility, and biodegradability. Pluronic F-127 is distinguished by its thermosensitivity, which allows it to retain encapsulated cells in its matrix and promotes subsequent cell attachment within the defective region [8]. Pluronic F-127 has also been demonstrated to boost cell adhesion and collagen synthesis, resulting in increased revascularization [9]. Brunet-Maheu et al. demonstrated that Pluronic F-127 has an optimal cell dispersion in liquid and is easily manipulatable in the solid form [10]. Furthermore, the FDA has approved its usage in humans. Pluronic F-127 offers an extensive array of uses, such as medication delivery and cell encapsulation [11].

Alginate is a non-toxic, biodegradable, and non-immunogenic linear polysaccharide comprised of guluronic and mannuronic acids that occurs naturally. Additionally, to its remarkable biocompatibility, it is a marine product derivative of the cell walls of brown algae that produces a hydrogel in moderate circumstances [12]. As a result of these factors, many biomaterials researchers and bioengineers use alginate as a constituent in the development and manufacturing of bioinks [13]. Hydrogels have been manufactured employing multilayer, composite, and interconnected polymeric networks (IPN) to overcome the limits of single-component hydrogels, endowing the gels with better and novel functionality. Polymeric network hydrogels have been discovered to have tremendous mechanical properties and can accumulate a significant amount of water while preserving their structure, functionality, and durability [14].

Polymeric blends and crosslinked Pluronic have been found to improve durability and gelation behavior. Unfortunately, few investigations on the reversibility of hydrogels and their applicability have been conducted [15]. The objective of this study was to create a thermoreversible hydrogel-based bioink composed of Pluronic F127 and alginate that may be used to construct scaffold structures utilizing 3D printing technology. Conventional bioinks' structural, thermal, and degrading qualities were anticipated to be improved by the bioink. The structures were then printed with the bioink, and their printability, cell proliferation, and cell survival were assessed.

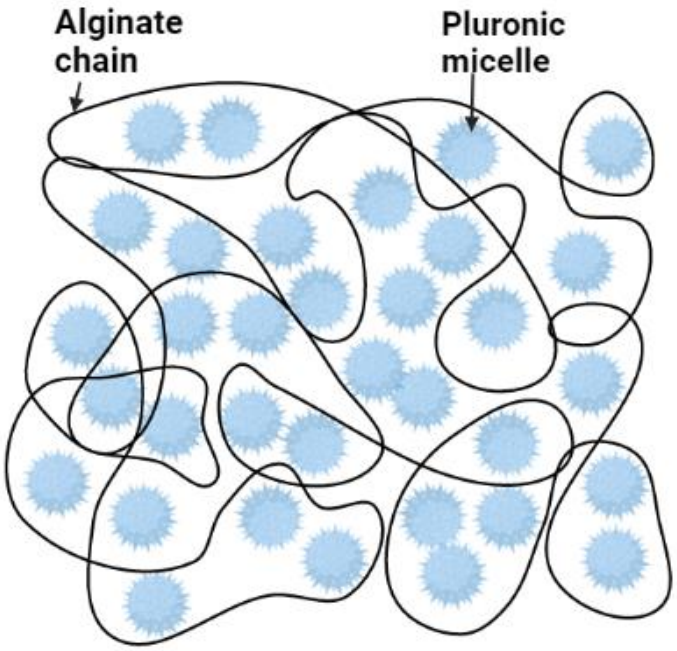

Figure 1: Schematic representation of Pluronic/Alginate hydrogel. Pluronic micelles, organizing in three-dimensional domains, in the alginate network. Created using Biorender.com

II. MATERIALS AND METHODS

A. *Materials*

Pluronic F127, sodium alginate, calcium chloride, Dimethyl sulfoxide (DMSO) were procured from Sigma-Aldrich. Phosphate-buffered saline (PBS), 3-(4,5-dimethylthiazol-2-yl)-2,5-diphenyl-tetrazolium bromide (MTT), Dulbecco's modified Eagle's medium (DMEM), fetal bovine serum (FBS), penicillin, and trypsin-ethylenediaminetetraacetic acid (EDTA) (0.25%) were purchased from Gibco. Deionized water was obtained using a Millipore water purification system.

B. *Preparation of polymeric blended hydrogels*

C.
Thermosensitive Pluronic PF127 and sodium alginate were formed into a matrix to create the Pluronic integrated sodium alginate (PF127/SA) hydrogels. In a nutshell, a physical combination of PF127 and SA was created by dissolving with various concentrations (% w/w) of PF127/SA of 25/1, 25/2, 30/1, and 30/2 in 4 °C PBS (previously cooled) constantly swirling to guarantee total dissolution. The resultant mixture was then kept at 4 °C.

D. *Sol-Gel phase transition behavior*

Using the tube-inversion approach, the phase transition of the PF127-blended SA have been examined [16]. Initially, different hydrogel concentrations were prepared with PF127/SA (% w/w) of 25/1, 25/2, 30/1, and 30/2. The following approach was then used to track the behavior of the solution to gel transition. At 4 °C and 37 °C, 1 ml of the homogenous solution was positioned in a vial test tube.

E. *In Vitro cytotoxicity test (MTT Assay)*

The PF127/SA hydrogels were tested for cytotoxicity, after gelation, was assessed by utilizing the MTT assay using NIH 3T3 fibroblast cells grown in DMEM supplemented with 10% FBS, 1% penicillin-streptomycin, at 37 °C in a humidified atmosphere of 5% CO_2. Different concentrations of gel were added to the wells as a thin coating and crosslinked with $CaCl_2$. 3T3 cells were seeded on the crosslinked gel in a 12-well plate at 5×10^3 cells/well, and incubated overnight. After incubating the cells on the crosslinked gel, the cells were incubated with MTT (0.5 mg/mL) for 4 h. DMSO was then added to the supernatant medium to break down the formazan crystals produced by the viable cells. ELISA plate reader was used to determine the absorbance at 570 nm.

F. *Cell viability assay*

Employing the live/dead assay, which is a two-color fluorescent dye assay that differently tags cells that are alive as well as dead, the cell viability of seeded cells on scaffolds was evaluated. By combining 1.5 µl of PI and 0.5 µl of Calcein-AM in 1 ml of Assay buffer, an initial solution of live/dead reagent was obtained. The scaffolds received 100 µl of live/dead solution,

which was then incubated for 30 min at room temperature. The Nikon Eclipse-TE2000-U fluorescent microscope was used for observing the well plate.

.

III. RESULTS

A. Sol-Gel transition

The tube inversion method is a frequently utilized technique to examine the Sol-Gel transition of the gels [16]. The PF127/SA hydrogel with various concentrations was prepared (% w/w) (25/1, 25/2, 30/1, and 30/2). The hydrogels displayed a solution state at 4 °C and quickly formed gel at 37 °C (7 min) (Fig 2). Upon increasing temperature to levels close to physiological temperatures, Pluronic go through a Sol-Gel transition. Increasing the ambient temperature of these non-ionic materials results in a decrease in the critical micelle concentration(CMC) and a rise in the micelle volume fraction, which surpasses the threshold of criticality and causes micellar crystallization and the onset of a self-sustaining gel state at higher temperatures [17,18].

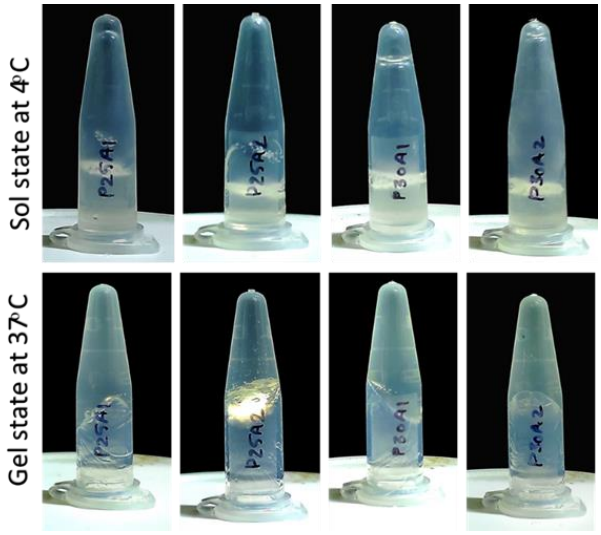

Figure 2: Reversible thermosensitive hybrid hydrogel developed by combining sodium alginate and pluronic undergoes a sol-gel transition. The hybrid hydrogel made up of various PF127/SA (% w/w) concentrations (25/1, 25/2, 30/1, and 30/2) was then evaluated using the tube-inversion technique.

B. 3D printed structures

The PF127/SA hydrogels are composed of 2 forms of crosslinked systems generated by a thermosensitive procedure and calcium ion addition. The quantity of polysaccharide, SA, in the polymeric, composite hydrogel altered its thermosensitivity. Because the bioprinting window affects the use of a bioink, the formulation of bioinks must be precisely explored [19]. Despite the ease and low cost of making calcium alginate hydrogels, network variability within a typical calcium alginate hydrogel leads to various pore sizes [8]. Calcium chloride and alginate's intermolecular crosslinking makes the gel less likely to break down in the body, which strengthens its structural robustness. An additional disadvantage of calcium alginate hydrogels is their high permeability, which results in limited carrier molecule absorbency [11].

A nozzle size of 25G, an extrusion pressure of 65 kPa, and a printing speed of 50 mm/s at 37 °C produced a 100% full scaffold print (Fig 3). In all printability criteria tested, these printing conditions did produce the best results. It was established by eyeballing, in conjunction with significant scaffold rating techniques, were an equally essential component to evaluate when establishing the ideal printing settings. The generated self-sustaining 3D shapes were additionally preserved by crosslinking the alginate chains with a $CaCl_2$ solution. The increased temperature induced a spur-of-the-moment sol-gel changeover facilitated by the F127 portion of the fabricated layers.

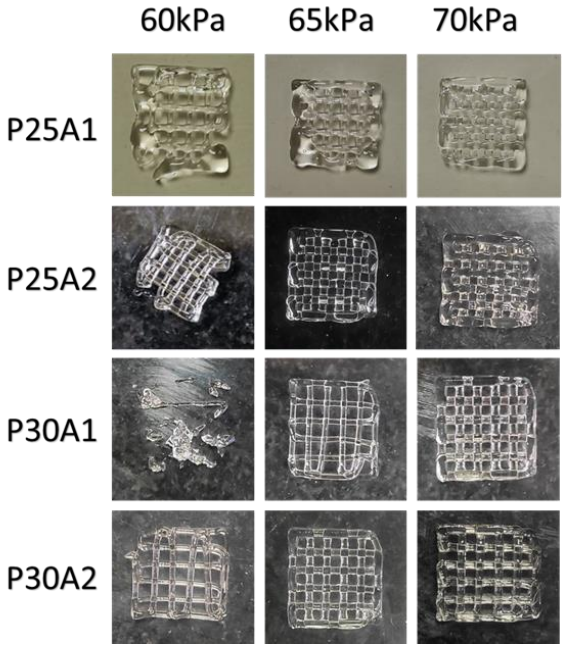

Figure 3: Representative images of the 3D printed grid structures of PF127/SA hydrogel at various concentrations (25/1, 25/2, 30/1 and 30/2) and extrusion pressures (60kPA, 65kPa and 70kPa).

C. Cell proliferation and viability (MTT assay)

Both SA and PF127 are nontoxic polymeric materials with USA FDA approval and are often employed in several therapeutic applications. nevertheless, due to the possible impact of the crosslinking calcium ions on cell proliferation and endurance, the damaging effects of hydrogels must be carefully taken into account before conducting in vivo research. The MTT test was used to quantitatively measure the proliferation of cells. The proliferation of the 3T3 cells was equivalent to that of tissue culture polystyrene dishes (TCPS) at all concentrations, demonstrating the compatibility of hydrogel with the cells. The biocompatibility of the polymers after gelation was confirmed by the noticeably high cell viability (Fig. 4) found after seeding 3T3 cells on PF127/SA hydrogel, which satisfies the requirements for the biological analysis. In comparison to other scaffolds, P25A2 demonstrated comparable cell growth with the control.

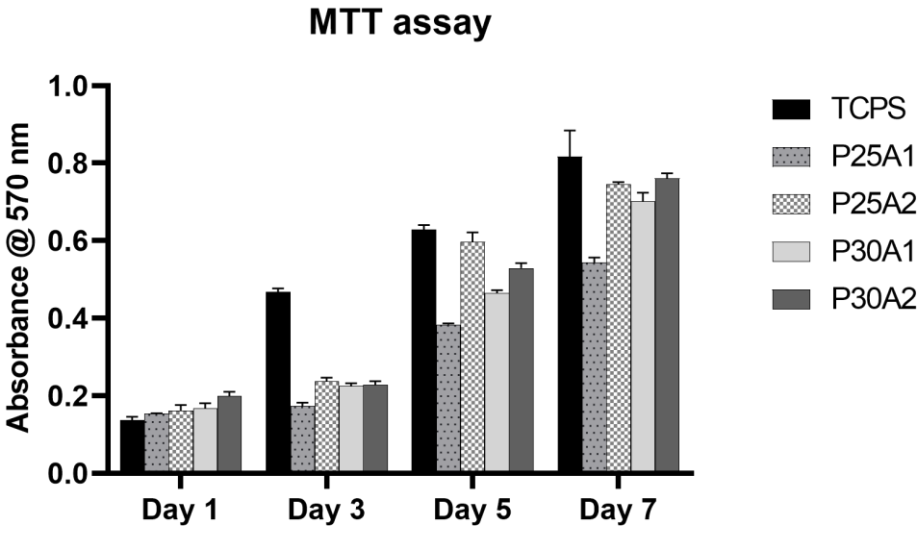

Figure 4: MTT assay showing proliferation of 3T3 cells on scaffolds of various concentrations of PF127/SA hydrogel at various time points.

D. Cell viability assay

A live/dead experiment was also carried out to evaluate the vitality of hydrogels after 24 hours of seeding at different time periods (Day 1, 3, and 5), and images were captured using a fluorescence microscope. Since there were fewer dead cells on each scaffold than there were living cells, it was determined that none of the scaffolds were harmful to 3T3 cells. P25A2 displayed better cell viability with fewer dead cells than other scaffolds.

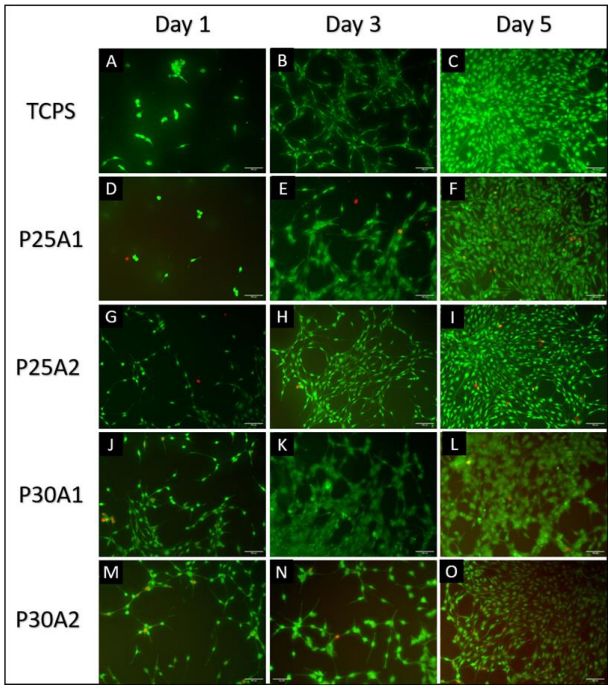

Figure 5: Live/dead assay (green-live cells and red-dead cells) 3T3 cells seeded on TCPS (A-C), P25A1 (D-F), P25A2 (G-I), P30A1 (J-L), and P30A2 (M-O) at various time points (Day 1, 3 and 5). P25A2 scaffold displyed better cell viability compared to other concentrations.

IV. CONCLUSION

In this study, a reversible thermosensitive composite hydrogel was developed as a printable biomaterial ink for the encapsulation of cells and 3D print the scaffolds for tissue engineering applications. Structural integrity depends heavily on the hybrid network hydrogel's reversible properties and its blend of calcium alginate and thermally cross-linked PF127. The printed structures displayed greater cell proliferation and cell viability similar to that of TCPS control. The PF127/SA hydrogel offers a promising combination as a bioink for various tissue engineering applications.

ACKNOWLEDGMENT

"We would like to acknowledge Department of Science & Technology for SERB-POWER research grant (SPG/2021/003703) for the financial support. Authors would also like to extend thanks to the Manipal Institute of Regenerative Medicine, MAHE for the infrastructural support".

REFERENCES

[1] S. A. Wilson, L. M. Cross, C. W. Peak, and A. K. Gaharwar, "Shear-Thinning and Thermo-Reversible Nanoengineered Inks for 3D Bioprinting," ACS Applied Materials & Interfaces, vol. 9, no. 50, pp. 43449-43458, 2017/12/20 2017, doi: 10.1021/acsami.7b13602.

[2] J. Gopinathan and I. Noh, "Recent trends in bioinks for 3D printing," Biomaterials research, vol. 22, pp. 1-15, 2018.

[3] M. C. Catoira, L. Fusaro, D. Di Francesco, M. Ramella, and F. Boccafoschi, "Overview of natural hydrogels for regenerative medicine applications," Journal of Materials Science: Materials in Medicine, vol. 30, no. 10, p. 115, 2019/10/10 2019, doi: 10.1007/s10856-019-6318-7.

[4] G. Tang et al., "Advances of Naturally Derived and Synthetic Hydrogels for Intervertebral Disk Regeneration," (in eng), Frontiers in bioengineering and biotechnology, vol. 8, pp. 745-745, 2020, doi: 10.3389/fbioe.2020.00745.

[5] R. S. Stowers, "Advances in Extracellular Matrix-Mimetic Hydrogels to Guide Stem Cell Fate," Cells Tissues Organs, vol. 211, no. 6, pp. 703-720, 2022, doi: 10.1159/000514851.

[6] X. Cui et al., "Advances in Extrusion 3D Bioprinting: A Focus on Multicomponent Hydrogel-Based Bioinks," Advanced Healthcare Materials, https://doi.org/10.1002/adhm.201901648 vol. 9, no. 15, p. 1901648, 2020/08/01 2020, doi: https://doi.org/10.1002/adhm.201901648.

[7] I. R. Schmolka, "Artificial skin I. Preparation and properties of pluronic F‐127 gels for treatment of burns," Journal of biomedical materials research, vol. 6, no. 6, pp. 571-582, 1972.

[8] H.-Y. Chou, C.-C. Weng, J.-Y. Lai, S.-Y. Lin, and H.-C. Tsai, "Design of an Interpenetrating Polymeric Network Hydrogel Made of Calcium-Alginate from a Thermos-Sensitive Pluronic Template as a Thermal-Ionic Reversible Wound Dressing," Polymers, vol. 12, no. 9, doi: 10.3390/polym12092138.

[9] K. M. Park, S. Y. Lee, Y. K. Joung, J. S. Na, M. C. Lee, and K. D. Park, "Thermosensitive chitosan–Pluronic hydrogel as an injectable cell delivery carrier for cartilage regeneration," Acta Biomaterialia, vol. 5, no. 6, pp. 1956-1965, 2009/07/01/ 2009, doi: https://doi.org/10.1016/j.actbio.2009.01.040.

[10] J.-M. Brunet-Maheu, J. C. Fernandes, C. A. V. De Lacerda, Q. Shi, M. Benderdour, and P. Lavigne, "Pluronic F-127 as a cell carrier for bone tissue engineering," Journal of biomaterials applications, vol. 24, no. 3, pp. 275-287, 2009.

[11] J. Cao et al., "Nitric Oxide-Releasing Thermoresponsive Pluronic F127/Alginate Hydrogel for Enhanced Antibacterial Activity and Accelerated Healing of Infected Wounds," Pharmaceutics, vol. 12, no. 10, doi: 10.3390/pharmaceutics12100926.

[12] J. L. Bron, L. A. Vonk, T. H. Smit, and G. H. Koenderink, "Engineering alginate for intervertebral disc repair," Journal of the mechanical behavior of biomedical materials, vol. 4, no. 7, pp. 1196-1205, 2011.

[13] F. Abasalizadeh et al., "Alginate-based hydrogels as drug delivery vehicles in cancer treatment and their applications in wound dressing and 3D bioprinting," Journal of biological engineering, vol. 14, pp. 1-22, 2020.

[14] S. Eswaramma and K. S. V. K. Rao, "Synthesis of dual responsive carbohydrate polymer based IPN microbeads for controlled release of anti-HIV drug," Carbohydrate Polymers, vol. 156, pp. 125-134, 2017/01/20/ 2017, doi: https://doi.org/10.1016/j.carbpol.2016.09.023.

[15] M. Abrami et al., "Physical characterization of alginate-Pluronic F127 gel for endoluminal NABDs delivery," (in eng), Soft Matter, vol. 10, no. 5, pp. 729-37, Feb 7 2014, doi: 10.1039/c3sm51873f.

[16] R. Prabhu, C. Yelamaggad, and G. Shanker, "Self-organisation properties of homomeric dipeptides derived from valine," Liquid Crystals, vol. 41, 02/28 2014, doi: 10.1080/02678292.2014.896484.

[17] B. Jeong, S. W. Kim, and Y. H. Bae, "Thermosensitive sol–gel reversible hydrogels," Advanced Drug Delivery Reviews, vol. 54, no. 1, pp. 37-51, 2002/01/17/ 2002, doi: https://doi.org/10.1016/S0169-409X(01)00242-3.

[18] J. P. K. Armstrong, M. Burke, B. M. Carter, S. A. Davis, and A. W. Perriman, "3D Bioprinting Using a Templated Porous Bioink," Advanced Healthcare Materials, https://doi.org/10.1002/adhm.201600022 vol. 5, no. 14, pp. 1724-1730, 2016/07/01 2016, doi: https://doi.org/10.1002/adhm.201600022.

[19] M. Hibbert, J. M. Viljoen, and L. H. du Plessis, "Print parameter optimisation for a Pluronic F-127 and alginate hybrid hydrogel," Bioprinting, vol. 30, p. e00257, 2023/04/01/ 2023, doi: https://doi.org/10.1016/j.bprint.2022.e00257.

YOLO in Digital Pathology: A Comprehensive Review

Shivani H Tantri
Department of Biomedical Engineering
Manipal Institute of Technology

Manipal Academy of Higher Education
Manipal, India
shivanitantri@gmail.com

Liora Dsilva
Department of Biomedical Engineering
Manipal Institute of Technology

Manipal Academy of Higher Education
Manipal, India
lioradsilva33@gmail.com

Niranjana Sampathila*
Department of Biomedical Engineering
Manipal Institute of Technology

Manipal Academy of Higher Education
Manipal, India
niranjana.s@manipal.edu

*Correspondence

***Abstract*— Digital pathology, a field gaining momentum in healthcare systems, is becoming increasingly popular with emerging whole-slide imaging technologies. Digitizing whole-slide images of histopathological specimens has led to the advent of Artificial Intelligence (AI) in digital pathology. The benefits of applying AI to this domain include standardization and reproducibility, increased diagnostic accuracy, greater availability of expertise, and increased efficiency. Moreover, the onset of general-purpose object detection algorithms like YOLO (You Only Look Once) has made detection and classification procedures in diagnostics easier. This review aims to discuss the application of YOLO in digital pathology. It briefly describes the different YOLO versions released thus far and how each has been utilized to aid clinical practice and diagnosis.**

Keywords*— *YOLO, object detection, digital pathology, classification, blood smear, microscopic image.

I. INTRODUCTION

Digital pathology involves digitizing histopathological glass slides utilizing whole-slide image scanners and analyzing these digital images using image analysis techniques for detection, segmentation, and classification. Many of these image analysis techniques involve quantifying or grading tissues, which requires the identification of histologic components. Therefore, developing efficient and robust digital pathology image analysis algorithms may be essential. This is accomplished by using various computational techniques, such as AI and deep learning techniques, which contribute to improving diagnostic accuracy, supporting the exploration and definition of new diagnostic and prognostic criteria, and assisting pathology laboratories in coping with increasing workloads and a lack of expertise [1].

Several researchers have applied image processing and computer vision techniques to create computer-aided diagnosis methods. These have been beneficial in determining the location of diseases and their spatial extent on digitized tissue sections. Computer vision feature-based methods are used with deep learning techniques, which employ architectures that can be constructed using convolutional networks to learn from image data. These convolutional neural network models offer higher flexibility because of their ability to be re-trained using a custom dataset for any application. They obtain higher levels of accuracy when classifying, detecting, and segmenting digital histopathological images, such as identifying nuclei and glands or recognizing cancer. With enough data to train a model, the accuracy is frequently on par with or better than that of experienced physicians [2], [3]. Chen et al. developed an AI model using deep learning to detect leukemic cells quickly, cheaply and more accurately from a microscopic blood smear image. The model accurately identified whether the image contained healthy or cancerous cells, thus demonstrating the implementation of object detection models for improving the efficiency of a blood cancer diagnosis. Fig.1 shows blood smear images from Acute Lymphoblastic Leukemia (ALL) patients and healthy individuals obtained from ALL-IDB (Acute Lymphoblastic Leukemia Image Database for Image Processing) blood samples [4]. This is a public and accessible dataset of microscopic images of blood samples focused on Acute Lymphoblastic Leukemia.

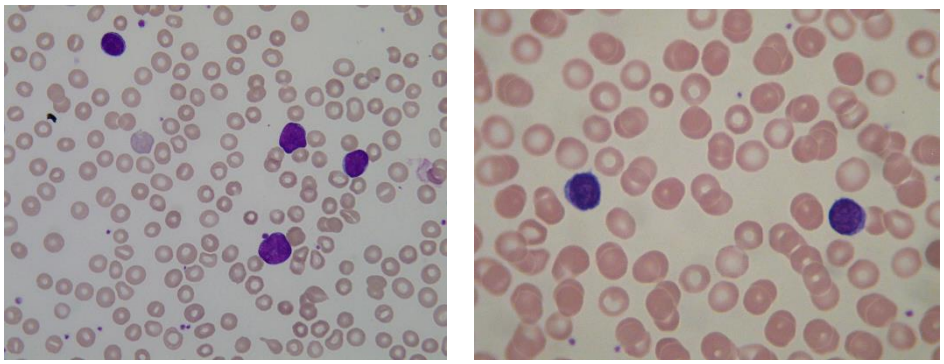

Fig. 1. An image from an ALL patient on the left and an image from a healthy individual on the right [5].

The goals of object classification and object detection, respectively, are to determine the type of an object in an image and to determine both type and location simultaneously. An object detector locates the presence of various objects with a labeled bounding box and subsequently classifies the located objects within the input image. The two types of object detectors are two-stage and single-stage object detectors. Two-stage detectors emphasize selective range proposal strategies for complex architectures, while single-stage detectors focus on all spatial ranges for possible object detection for relatively simple architectures. In general, the detection accuracy of a two-stage detector is superior to that of a single-stage object detector [6]. However, the inference time of the single-stage detector is better than the corresponding detector. One such single-stage object detector is the You Only Look Once (YOLO) object detection algorithm, which deals with problems using regression analysis based on a darknet deep learning framework. The model's compact size and high calculation speed form the basis of the YOLO target detection algorithm. This algorithm's speed can be attributed to the fact that it only needs to transfer the image to the network to obtain the final detection result [6]. Herein, we briefly discuss the original YOLO network architecture, its subsequent versions, and how each version outperformed its predecessor. We also briefly explain the object detection method and examine existing literature on YOLO applications in digital pathology.

II. YOLO Architecture

The design of YOLO includes the Darknet architecture that processes all image features. The network consists of 24 convolutional layers followed by two fully connected layers that predict bounding boxes for objects. The network's initial convolutional layers extract image features, whereas the fully connected layers predict the coordinates and output probabilities. The GoogLeNet model, a network with 22 layers deep, used for image classification, served as an inspiration for the network architecture. Instead of the inception modules used by GoogLeNet, 1 × 1 reduction layers followed by 3 × 3 convolutional layers are used. The feature space from preceding layers is reduced by alternating 1 × 1 convolutional layers. A 224 × 224 input image was utilized to train the feature extractor using the first 20 convolution layers. Following the addition of the final four convolution layers and the two fully connected layers, the input image's resolution concomitantly improved to 448 × 448 to be used as an object detector. The network's final output is the 7 × 7 × 30 tensor of predictions [7].

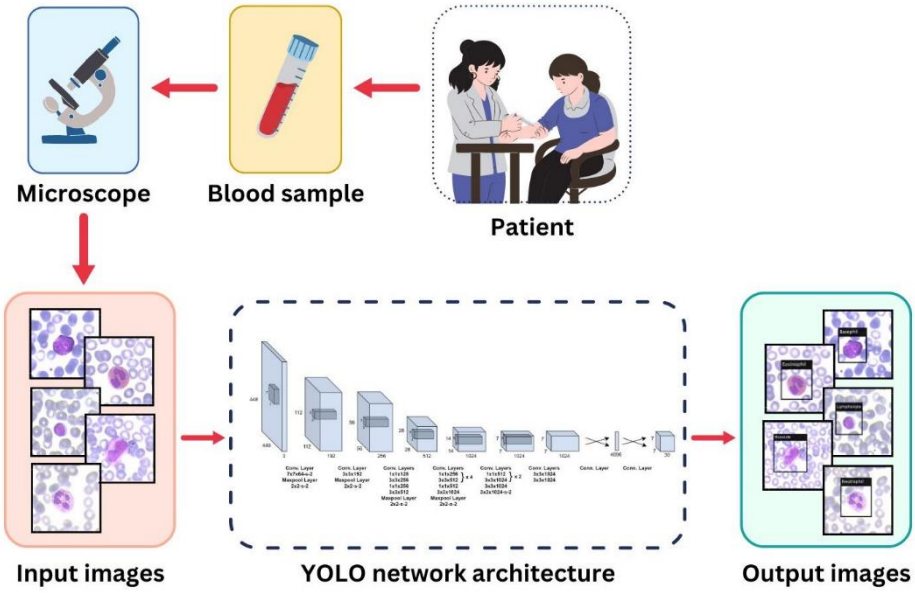

Fig. 2. YOLO-based system for the detection and classification of different types of leukocytes.

III. YOLO Methodology

The image is divided into S × S grid cells in the object detection process. Each grid cell of the image predicts bounding boxes along with their dimensions and positions, class conditional probabilities, and the probability of containing an object in a grid cell. Image classification and object localization techniques are applied to each grid cell, and each cell is labelled. The algorithm checks each grid cell separately and marks the label and bounding boxes of the cell with an object in it [7]. Grid cells without objects have labels that are marked as zero. For an object to be detected by a bounding box, its center should lie within the bounds of that box. Since it is possible for many objects to have their centers in the same bounding box, anchor boxes are

employed in order to represent the bounding boxes that correspond to a single grid cell. Anchor boxes are bounding boxes that differ in size and shape and are selected after analyzing the dataset and the objects within the dataset. If multiple grid cells contain the same object, the irrelevant cells should be discarded to detect objects accurately. This can be achieved by using the methods of Intersection over Union (IoU) and Non-Max Suppression (NMS) [8]. Fig.2 shows an object detection and classification system using the original YOLO architecture to detect different types of WBCs. The LISC (Leukocyte Images for Segmentation and Classification) database is used to obtain the WBC images [9].

IV. EVOLUTION OF YOLO

YOLO has been released in 8 different versions (including the original). The most cutting-edge concepts from computer vision research have been improved and integrated into each version. In order to simplify the enormous run-time complexity of the region-based convolutional network (R-CNN) and the deformable part-based model (DPM), Redmon et al. developed the YOLO object detection network. Although YOLO outperformed these detection methods by a wide margin, it required further improvement.

YOLOv2, an improved version of the original YOLO, primarily focused on recall and localization improvements while maintaining classification accuracy [10]. This version replaced the fully connected layers used in YOLOv1 with an anchor box architecture to predict bounding boxes. Compared to the earlier YOLO version, the recall value was boosted by using anchor boxes. Additionally, YOLOv2 added a batch normalization layer, which enhanced detection performance and eliminated chances of overfitting.

However, because this version frequently had trouble detecting small objects, a newer version named YOLOv3 was proposed. YOLOv3 developed a better architecture where the feature extractor was a hybrid of YOLOv2, Darknet-53 (53 convolutional layers), and Residual networks (ResNet) [11]. This version handled multi-class prediction effectively because it used independent logistic classifiers for each class. It performed detections at three different scales, and this ability to detect at multiple scales helped it detect small objects more efficiently. However, it performed poorly on medium and large-sized objects.

Aly et al. compared the performance of YOLOv1, YOLOv2 and YOLOv3 models by using them for the detection of breast masses and their classification into malignant and benign lesions in full-field digital mammograms. Because anchor boxes were incorporated into the YOLOv2 model, this model produced better results than the YOLOv1 model. Moreover, the YOLOv3 model achieved excellent mass detection and classification results, with average precision for benign and malignant masses of 94.2% and 84.6%, respectively [12].

The next version, known as YOLOv4, aimed at developing better training procedures. Researchers inspired from a number of Bag-of-Freebies and Bag-of-Specials techniques to improve the object detector's accuracy without raising the inference cost. Apart from these adjustments, they introduced an additional technique for data augmentation, used genetic algorithms to select the optimal hyper-parameter values, and modified a few existing techniques to make their designs more efficient for training and detection [13]. Khandekar et al. implemented the YOLOv4 model for automated detection and classification of blast cells in blood smear samples to assist in the diagnosis of leukemia from microscopic images. Inference time and classification accuracy both improved as a result of their effort. The model could effectively detect and classify single and multiple blast cells in a given image and make predictions on images without prior pre-processing [14]. The YOLOv4 model has also been used to detect artifacts in whole slide images to ensure quality performance during clinical diagnosis, as mentioned by Hemmatirad et al. The authors proposed a YOLOv4 deep model to detect the presence of tissue folds, air bubbles, and ink markers, which adversely affect the quality of the output tissue image and the ensuing diagnosis [15].

Although YOLOv4 and its successor, YOLOv5, share a very similar architecture, YOLOv5 improves the application of trained neural networks in video processing applications. This model has a variety of network architectures, which are more flexible to use and have a very lightweight model size [16]. Even though it is as good as the YOLOv4 benchmark in terms of accuracy, it has some performance improvements like a user-friendly framework, easy-to-read code, and is faster than its previously proposed versions [17]. The later YOLO versions, YOLOv6 [18] and YOLOv7 [19] perform even better than YOLOv5, particularly when detecting small objects in densely packed environments.

Both these versions outperform the YOLOv5 model in object detection accuracy, training and classification speed. A paper by Chen et al. compared the performance of YOLOv5, YOLOv6 and YOLOv7 models for the real-time detection of ALL cells from microscopic blood smear images. However, in this study, the YOLOv5 model outperformed the YOLOv6 and YOLOv7 models regarding training-process accuracy. Among the two versions of YOLOv5 used, it was observed that the small version, called YOLOv5s, performed the best, achieving an accuracy of 97.2% [4].

The most recent version, YOLOv8, introduces a new framework; nevertheless, there has not been much work done in digital pathology, and this version is still in its early stages. Table 1 lists the various YOLO models that different authors have employed for multiple applications in digital pathology and the best outcomes they have attained.

TABLE I. MAXIMUM RESULTS OBTAINED BY DIFFERENT AUTHORS USING VARIOUS YOLO MODELS

Reference	Author	Objective	Model	Maximum results
[14]	Khandekar et al. (2021)	To detect blast cells automatically for the diagnosis of ALL	YOLOv4 YOLOv4	mAP = 95.57% mAP = 98.57%
[20]	Wang et al. (2021)	To detect and count eosinophils for the treatment of eosinophilic gastroenteritis	YOLOv3	mAP = 96.1% Precision = 97.6% Recall = 94.7%
[21]	Abdurahman et al. (2021)	To detect malaria parasites in microscopic blood smear images	YOLOv4-MOD YOLOv3-MOD2 YOLOv3-MOD1	mAP = 96.32% mAP = 96.14% mAP = 95.46%
[22]	Drioua et al. (2022)	To detect breast cancer from histopathology images	YOLOv5	Precision = 0.86 Recall = 0.77
[23s]	Huang et al. (2022)	To detect prostate cancer cells based on deep learning	YOLOv5	AP_{50} = 76.3

mAP, mean average precision; AP_{50}, average precision at IoU = 0.5

V. CONCLUSION

This review presents a comprehensive view of the YOLO object detection algorithm in the field of digital pathology. After providing a brief analysis of all the present versions of YOLO and how each version has been implemented for clinical diagnosis applications, it was observed that each version works better and more accurately than its predecessor.

The growing number of applications of object detection models, like YOLO, in computer-aided detection and diagnosis, proves it to be an innovative diagnostic tool that can assist clinicians in evaluating diseases in humans in the future. Nevertheless, there is room for improvement. Developing more efficient automated detection systems that allow patients to be diagnosed more quickly and accurately will undoubtedly push object detection in diagnostics towards a promising future.

REFERENCES

[1] P. Amerikanos and I. Maglogiannis, "Image Analysis in Digital Pathology Utilizing Machine Learning and Deep Neural Networks," *J Pers Med*, vol. 12, no. 9, p. 1444, 2022.

[2] A. Janowczyk and A. Madabhushi, "Deep learning for digital pathology image analysis: A comprehensive tutorial with selected use cases," *J Pathol Inform*, vol. 7, no. 1, 2016, doi: 10.4103/2153-3539.186902.

[3] A. Esteva *et al.*, "Deep learning-enabled medical computer vision," *npj Digital Medicine*, vol. 4, no. 1. 2021. doi: 10.1038/s41746-020-00376-2.

[4] E. Chen, R. Liao, M. Y. Shalaginov, and T. H. Zeng, "Real-time detection of acute lymphoblastic leukemia cells using deep learning," in *2022 IEEE International Conference on Bioinformatics and Biomedicine (BIBM)*, 2022, pp. 3788–3790.

[5] ALL-IDB Acute Lymphoblastic Leukemia Image Database for Image Processing. Available online: http://homes.di.unimi.it/scotti/all/

[6] T. Diwan, G. Anirudh, and J. v Tembhurne, "Object detection using YOLO: Challenges, architectural successors, datasets and applications," *Multimed Tools Appl*, pp. 1–33, 2022.

[7] J. Redmon, S. Divvala, R. Girshick, and A. Farhadi, "You only look once: Unified, real-time object detection," in *Proceedings of the IEEE conference on computer vision and pattern recognition*, 2016, pp. 779–788.

[8] M. Chandra Arya and A. Rawat, "A Review on YOLO (You Look Only One)-An Algorithm for Real Time Object Detection," *Journal of Engineering Sciences*, vol. 11, no. 6, 2020.

[9] LISC: Leukocyte Images for Segmentation and Classification. Available online: http://users.cecs.anu.edu.au/~hrezatofighi/Data/Leukocyte%20Data.htm

[10] J. Redmon and A. Farhadi, "YOLO9000: Better, faster, stronger," in *Proceedings - 30th IEEE Conference on Computer Vision and Pattern Recognition, CVPR 2017*, 2017, vol. 2017-January. doi: 10.1109/CVPR.2017.690.

[11] J. Redmon and A. Farhadi, "Yolov3: An incremental improvement," *arXiv preprint arXiv:1804.02767*, 2018.

[12] G. H. Aly, M. Marey, S. A. El-Sayed, and M. F. Tolba, "YOLO Based Breast Masses Detection and Classification in Full-Field Digital Mammograms," *Comput Methods Programs Biomed*, vol. 200, 2021, doi: 10.1016/j.cmpb.2020.105823.

[13] A. Bochkovskiy, C.-Y. Wang, and H.-Y. M. Liao, "Yolov4: Optimal speed and accuracy of object detection," *arXiv preprint arXiv:2004.10934*, 2020.

[14] R. Khandekar, P. Shastry, S. Jaishankar, O. Faust, and N. Sampathila, "Automated blast cell detection for Acute Lymphoblastic Leukemia diagnosis," *Biomed Signal Process Control*, vol. 68, 2021, doi: 10.1016/j.bspc.2021.102690.

[15] K. Hemmatirad, M. Babaie, M. Afshari, D. Maleki, M. Saiadi, and H. R. Tizhoosh, "Quality Control of Whole Slide Images using the YOLO Concept," in *2022 IEEE 10th International Conference on Healthcare Informatics (ICHI)*, 2022, pp. 282–287.

[16] M. Horvat and G. Gledec, "A comparative study of YOLOv5 models performance for image localization and classification," in *Central European Conference on Information and Intelligent Systems*, 2022, pp. 349–356.

[17] M. Maity, S. Banerjee, and S. S. Chaudhuri, "Faster r-cnn and yolo based vehicle detection: A survey," in *2021 5th international conference on computing methodologies and communication (ICCMC)*, 2021, pp. 1442–1447.

[18] C. Li *et al.*, "YOLOv6: A single-stage object detection framework for industrial applications," *arXiv preprint arXiv:2209.02976*, 2022.

[19] C.-Y. Wang, A. Bochkovskiy, and H.-Y. M. Liao, "YOLOv7: Trainable bag-of-freebies sets new state-of-the-art for real-time object detectors," *arXiv preprint arXiv:2207.02696*, 2022.

[20] X. Wang, Y. Che, N. Jiang, W. Chen, and L. Lan, "Eosinophil Detection with Modified YOLOv3 Model in Large Pathology Image," in *Proceedings - 2021 International Conference on Computer Information Science and Artificial Intelligence, CISAI 2021*, 2021. doi: 10.1109/CISAI54367.2021.00019.

[21] F. Abdurahman, K. A. Fante, and M. Aliy, “Malaria parasite detection in thick blood smear microscopic images using modified YOLOV3 and YOLOV4 models,” *BMC Bioinformatics*, vol. 22, no. 1, pp. 1–17, 2021.

[22] W. R. Drioua, N. Benamrane, and L. Sais, “Breast Cancer Detection from Histopathology Images Based on YOLOv5,” in *2022 7th International Conference on Frontiers of Signal Processing (ICFSP)*, 2022, pp. 30–34.

[23] H. Huang, Z. You, H. Cai, J. Xu, and D. Lin, “Fast detection method for prostate cancer cells based on an integrated ResNet50 and YoloV5 framework,” *Comput Methods Programs Biomed*, vol. 226, p. 107184, 2022.

Survey on various approaches and application of Machine learning algorithms for Medical Diagnosis of heart abnormalities

Shreeraksha

Department of Computer Science and Engineering
Shri Madhwa Vadiraja Institute of Technology and Management, Bantakal
shreeraksha.19cs091@sode-edu.in

Shrutha V Bhat

Department of Computer Science and Engineering
Shri Madhwa Vadiraja Institute of Technology and Management, Bantakal
shrutha.19cs094@sode-edu.in

Thejas S S

Department of Computer Science and Engineering
Shri Madhwa Vadiraja Institute of Technology and Management, Bantakal
tejas.19cs106@sode-edu.in

Vikram G T

Department of Computer Science and Engineering
Shri Madhwa Vadiraja Institute of Technology and Management, Bantakal
vikram.19cs116@sode-edu.in

Ms. Savitha Shenoy
Assistant Professor(Senior)
Department of Computer Science and Engineering
Shri Madhwa Vadiraja Institute of Technology and Management, Bantakal
savitha.cs@sode-edu.in

***Abstract* - heart disease, which includes illnesses like coronary artery disease and chronic heart failure, is the main cause of death worldwide. Due to the limits of conventional clinical approaches for diagnosis, researchers have developed machine learning and data mining techniques for faster and more accurate detection. This study intends to assess various modalities, such as medical characteristics, visuals, and ECG, for detecting heart problems.**

Keywords – Heart disease, Cardiovascular Disease, Machine learning.

I. INTRODUCTION

According to the World Health Organisation, cardiovascular disease (CVD) will account for 32% of all deaths globally in 2019. Early heart abnormality detection is essential to averting major consequences and enhancing patient outcomes. Machine learning (ML) methods offer a dependable, economical, and effective way to find heart problems. Electrocardiograms (ECGs), pictures, and medical feature-based data are the three basic modalities for diagnosing heart disease. Based on these modalities, ML techniques for diagnosing heart disease have been thoroughly researched. Medical feature-based data can be used to train machine learning algorithms to forecast a patient's likelihood of developing heart disease. While ECG-based approaches can find abnormalities in the electrical activity of the heart, image-based approaches can find anomalies in cardiac structure and function. ML-based diagnostic systems can offer a more precise and thorough evaluation of a patient's cardiovascular health by merging data from many modalities. For a lower fatality rate and improved decision-making for future treatment and prevention, early detection of cardiac disease using a prediction model is advised. By enhancing patient outcomes, lowering healthcare costs, and enabling more effective use of healthcare resources, the application of ML in the diagnosis of cardiovascular disease has the potential to revolutionise healthcare.

II. LITERATURE REVIEW

Mihir Patel et al. [1], aims to predict heart disease using machine learning algorithms. The study involved collecting data from patients who had undergone a cardiac examination, and various machine learning algorithms such as Decision Tree, Logistic regression, Random Forest, Naive Bayes, and K-Nearest Neighbor were applied to the dataset to determine which algorithm was most accurate in predicting the presence of heart disease. The results of the study showed that the Logistic regression algorithm had the highest accuracy in predicting heart disease, with an accuracy rate of 92%. Additionally, the researchers found that factors such as age, gender, cholesterol levels, and blood pressure were the most significant predictors of heart disease. The study highlights the potential of using machine learning algorithms to predict heart disease accurately, which could help in the early diagnosis and treatment of the disease, thus improving patient outcomes. The researchers suggest that further studies could be conducted to explore the use of other machine learning algorithms or combining multiple algorithms to improve the accuracy of the prediction models.

Yan Fang et al. [2] explores the use of a radial basis function (RBF) neural network for classifying electrocardiogram (ECG) signals to diagnose heart disease. The study aimed to evaluate the performance of the RBF neural network in detecting the presence of heart disease in ECG signals. The study collected ECG signal data from patients with and without heart disease and used feature extraction techniques to extract relevant features from the ECG signals. The extracted features were then used as inputs to the RBF neural network, which was trained to classify the ECG signals as either normal or abnormal. The results of the study showed that the RBF neural network had a high accuracy rate of 95.7% in classifying ECG signals to diagnose heart disease. The researchers also compared the performance of the RBF neural network with other machine learning algorithms such as the support vector machine and the backpropagation neural network and found that the RBF neural network outperformed these algorithms. The study highlights the potential of using RBF neural networks for diagnosing heart disease based on ECG signals. The researchers suggest that future studies could explore the use of larger datasets and additional feature extraction techniques to improve the accuracy of the classification models. Overall, the study provides promising results for the use of machine learning algorithms in the early diagnosis of heart disease.

Dimitri Grun et al. [3] aims to analyze the effectiveness of artificial intelligence in identifying heart failure through electrocardiogram (ECG) data. The study involved analyzing various published research studies that have used AI algorithms to identify heart failure through ECG data. The researchers analyzed 31 studies and found that AI algorithms have an overall sensitivity of 81% and specificity of 86%, which is a significant improvement compared to traditional methods. The study also found that the accuracy of the AI algorithm depends on various factors, such as the size and quality of the data set, the type of algorithm used, and the characteristics of the patient population. The researchers concluded that AI algorithms have the potential to improve the accuracy and efficiency of identifying heart failure through ECG data. However, further research is needed to optimize the algorithms and validate their effectiveness in clinical settings. Overall, this research paper highlights the promising role of AI in improving the diagnosis and management of heart failure.

M.V. Prasad et al. [4] aims to predict cardiac disease using Machine Learning (ML) and Deep Learning (DL) techniques by analyzing the Electrocardiogram (ECG) signals of patients. ECG is a commonly used non-invasive diagnostic tool to assess the heart's electrical activity and is crucial for diagnosing and managing cardiac diseases. The study uses a dataset of ECG signals collected from patients with and without cardiac disease. The authors preprocess the data to remove noise and artifacts and extract features using wavelet decomposition. They then apply several ML and DL techniques such as Decision Tree, Support Vector Machine, Random Forest, and Convolutional Neural Network to classify the ECG signals and predict the presence of cardiac disease. The results show that the DL techniques outperform the ML techniques in terms of accuracy, sensitivity, specificity, and F1-score. The study concludes that DL techniques can be effectively used for the early detection and diagnosis of cardiac disease, which can lead to better patient outcomes and improved healthcare management. The research paper presents a novel approach to predict cardiac disease by analyzing ECG signals using ML and DL techniques, which can potentially improve the diagnosis and treatment of cardiac diseases.

Naive Bayes technique has been utilised with image processing by Mamta Rani et al. [5]. It illustrates how the framework operates when the Naive Bayes algorithmic programme of patient learning is used. The programme uses this information to feed a Nave Bayes algorithmic programme after retrieving the patient's record from the interface. Possibilities will be identified and each credit will be handled using the Naive Bayes algorithm. At that point, each claim will be examined, and based on the results, the information on risk will be provided. The yields will be included in the data, which will improve the learning environment. The accuracy of this system was 85% during the validation phase, 85% during the testing phase, and 79% on average during the regression phase.

An overview of the many strategies used by researchers to predict cardiac abnormalities is presented by Tanvi Dhamdhere et al. [6]. Treatment and early detection of cardiac arrhythmia have the potential to save patients' lives. Since ECG signals are time-series data, we can successfully predict cardiac arrhythmia using cutting-edge machine learning techniques and large datasets. There are numerous techniques that can be used to find cardiac problems.

According to Ali Haider Khan et al. [7], SSD MobileNet V2 is a deep neural network architecture that was used to diagnose cardiovascular illness with good accuracy. The accuracy of the study's ECG picture processing to identify four significant cardiac anomalies was 98% on average. Although several cardiologists manually checked the proposed system's accuracy, due to differences in dataset and class types, it should not be directly compared to earlier research studies.

To identify R, P, and T peaks in ECG data, Saira Aziz et al. [8] have presented a fusion technique that makes use of FrFT and TERMA. The method was independent of cardiovascular disorders and outperformed TERMA in detecting the P and T waveforms. The research also describes a prototype wireless ECG diagnosis device that transmits and displays ECG signals on an Android smartphone. A later iteration of the app will incorporate the suggested algorithms.

M. H. Vafaie et al. [9] proposed a method for predicting cardiac illnesses based on ECG signal classification that employs a genetic-fuzzy system and an ECG signal dynamical model. The suggested solution combines the benefits of genetic and fuzzy systems to account for the complexity and unpredictability in ECG readings. The NARX model is utilised to extract significant characteristics from ECG data, and the genetic-fuzzy system is used for classification, with two specific fuzzy rules as examples. The suggested technique achieves 98.6% accuracy in properly categorising 296 out of 300 ECG signals, showing its potential utility in clinical situations. However, further validation on larger datasets is required to ensure the method's generalizability and practicality. In conclusion, the proposed method is a potential approach for enhancing the accuracy and efficiency of cardiac disease diagnosis by ECG signal classification.

A content-based image retrieval (CBIR) system for ECG reports is presented by Dr Naveen B et al. [10]. The system's goal is to help physicians diagnose cardiac disorders by retrieving similar ECG readings from a database quickly and accurately. The paper's methodology combines feature extraction techniques, similarity metrics, and indexing methodologies. The time and frequency domain features are retrieved from ECG signals, and the Euclidean distance is employed to quantify similarity. The suggested system employs the k-d tree data structure for indexing. The authors assess the system's performance using precision and recall measures, which quantify the system's accuracy in obtaining relevant ECG reports. The suggested CBIR system for ECG reports has a high accuracy, with precision and recall values ranging from 91% to 100%, according to the paper. These findings support the suggested system's ability to retrieve relevant ECG reports from a database. The authors conclude that the CBIR system has the potential to help clinicians diagnose cardiac problems and improve patient outcomes. However, additional validation and refinement of the system are required to improve its accuracy and usability in clinical settings.

Deep learning algorithms are used by Siddharth Mishra et al. [11] to digitise and diagnose ECG recordings. The authors examined 3200 ECG samples and converted pdf data to image format for additional analysis. The images were thresholders, which were used to extract the ECG signal without using the grid. A dataset of 255 binarization values with regard to a single image was constructed, and the characteristic curve of the ECG waveform was discovered to be a superior feature that increased binarization and diagnosis accuracy. Any ECG digitization must include a shadow removal algorithm and uniform luminance correction. The authors also created a DL model that could detect four different diseases: LBBB, RBBB, T-wave abnormalities, and STEMI. Class 3, which is LBBB, had the most misclassifications. According to the authors, obtaining the 1-D ECG signal from paper data opens up a new avenue for developing various digitising algorithms and automated diagnoses. This could be the most advantageous for persons living in rural areas. The research provides a unique method for ECG digitization and diagnosis, although it involves human thresholding and post-processing. Additional research is required to automate these steps and assess the method's feasibility in real-world clinical settings.

Isna Fatimatuz Zahra et al. [12] In the investigation mentioned in the text, a piezoelectric sensor and a temperature sensor are used to monitor a patient's breathing and body temperature, respectively. The sensors are linked to a microcontroller, which processes the data and wirelessly transmits it to a PC. Using the Delphi application, the data is then presented on the PC. When an irregularity in the parameter value is discovered, such as an indication of a heart attack, the doctor is automatically notified. An analogue signal conditioning circuit, consisting of a summing amplifier and a low pass filter, is included in the system. According to the circuit design results, the analogue half is made up of a piezoelectric sensor and a PSA circuit made up of a summing amplifier and a low pass filter, while the digital part is made up of a temperature sensor, a microcontroller, and a wireless module.

The method suggested by Shaik Farzana et al. [13] utilised various machine learning algorithms. Datasets for heart disease, including its contributing components, have been acquired from the UCI Machine Learning Repository and subjected to further categorization models. For predicting cardiac illness, the methodology uses five machine learning models: Support Vector Machine, Random Forest, KNN, Gaussian Naive Bayes, and Xg-Boost algorithms. 13 features, including age, gender, blood pressure, cholesterol, obesity, and cp, are used in the framework.

Pranav Madihalli et al. [14] has identified several approaches that have implemented the heart disease prediction paradigm that has been studied with detail in this research paper. These approaches have been effective in achieving their prescribed goals but have some drawbacks or limitations that need to be addressed.

Cardiologists were consulted to confirm the validity of the diagnostic criteria developed by Armin Yazdani et al. [15] for the diagnosis of coronary heart disease. The greatest confidence rating for predicting coronary heart disease was 98% in trials conducted using the UCI open dataset, which is often utilized in investigations. This appears to give a significant addition to the computation of electrical rankings with excellent predictors of coronary heart disease. Through the use of the calculated strength rankings of significant predictors on Weighted Associative Rule Mining in predicting coronary heart disease, they were able to extract significant rules from the assessment findings and carry out their work with the maximum degree of confidence.

III. METHODOLOGY

The research strategy that we used to create this publication is as follows. The problem statement was where we started first. We considered acting against heart disease. Our main goal is to identify several strategies and useful algorithms to identify heart disease. Then, we looked through related papers and publications. Subsequently an effort to analyze the information in each study is made and some conclusions are obtained.

Fig 1: Overall methodology block diagram

- **Collecting dataset:**
  A dataset refers to a compilation of information where the data is organized systematically. It can encompass diverse data types, ranging from arrays to tabulated records in a database. To engage in machine learning projects, a substantial volume of data is indispensable, as the absence of data hinders the training of ML/AI models. The process of gathering and readying the dataset holds utmost significance during the development of an ML/AI project.
- **Pre-processing:**
  Data preprocessing is an essential initial step in developing a machine learning model, involving the preparation of raw data to make it appropriate for analysis. It serves as a fundamental and crucial phase in any machine learning

project. Clean and well-structured data is not always readily available, necessitating the need for data preprocessing tasks. These tasks are indispensable in cleansing and organizing the data to ensure its suitability for subsequent operations..

- **Train set:**
  Upon completing the model construction, the subsequent step involves model training. The training process utilizes a designated subset of the dataset known as the trainset. In this subset, the expected output is already known, enabling the machine learning model to learn and optimize its performance based on this information.
- **Test set:**
  Following the training phase, model testing can be conducted, wherein a separate set of data, known as the test set, is utilized. The test set contains data that the model has never encountered before, allowing for the verification of its actual accuracy. Essentially, the test set serves as a subset of the dataset used to evaluate the machine learning model, enabling predictions to be made by the model based on this distinct dataset.
- **Learning Algorithm:**
  Machine Learning algorithms are software programs capable of autonomously learning from data, identifying concealed patterns, making predictions, and enhancing performance based on past experiences. Various algorithms serve different purposes in machine learning. For instance, simple linear regression finds utility in predictive tasks like stock market forecasts, while the KNN algorithm proves effective in classification problems.
- **Comparing Output:**
  Here we compare the actual outcome and expected outcome of the results.

IV. RESULTS AND DISCUSSION

In our analysis, we thoroughly examined the top 17 research papers from each modality, evaluating their accuracy and performance across different datasets. ECG-based machine learning (ML) techniques consistently demonstrated superior accuracy and performance compared to clinical feature-based approaches. Moreover, clinical feature-based and image-based ML methods experienced a decline in accuracy and performance when confronted with large datasets, while ECG-based models remained effective regardless of the dataset size. The nature of the data within a dataset emerged as a critical factor impacting the ML model's performance. The three modalities utilized diverse datasets, including ECG signals, images, and medical reports, resulting in varying data characteristics. Consequently, ECG-based ML models, utilizing signal data, achieved higher accuracy and performance compared to other modalities for predicting and detecting heart failure (HF) and cardiovascular disease (CVD).

Feature selection/extraction also plays a significant role in ML models, involving the identification of the most appropriate features from the feature space. This process reduces the feature space by eliminating irrelevant features, thereby enhancing the performance and accuracy of ML models. Feature selection is distinct from feature extraction. In feature selection, only the most influential features are chosen from the feature vector to improve accuracy, while feature extraction generates new features from the existing feature space, thereby boosting the accuracy of ML models. Therefore, effective feature processing is crucial in ML models, as it not only improves accuracy but also reduces computational costs.

Study	Input	Algorithm used	Accuracy
Mihir Patel et al. [1]	Clinical parameters	Linear regression	92%
Yan Fang et al. [2]	ECG signals	RBF neural network	95.7%
M.V. Prasad et al. [4]	ECG signals	CNN LSTM network	98.74%
Mamta Rani et al. [5]	ECG signals	Naive Bayes	85%
Ali Haider Khan et al. [7]	ECG Signals	SSD MobileNet V2	98.33%
Saira Aziz et al. [8]	ECG Signals	SVM	99.8%
		MLP	96.5%
Shaik Farzana et al. [13]	Clinical Parameters	Random Forest	88.52%
Senthilkumar Mohan et al. [16]	Clinical parameters	Gaussian Naive Bayes	82.25%
Sakshi Goel et al. [17]	Clinical parameters	Support vector machine	92.1%

Table 1: Result table

V. CONCLUSION

Cardiovascular illness can be predicted and treated in advance, saving the lives of patients. Given that ECG signals are time-collection records, we may forecast cardiovascular illnesses with great success by using large enough datasets and advanced machine learning techniques. This article provides an overview of the numerous techniques' researchers have used to predict cardiac abnormalities. In the recent years, a number of ML strategies were suggested for the prediction of CVD and HF; nevertheless, there are a few areas that researchers and experts also wish to investigate. We draw the conclusion from this study that the effective detection of CVD and HF depends on three essential components. First of all, ML-based systems may require a substantial amount of data. At first, data may be rather substantial in the case of ML-based fully automatic identification of heart disease, particularly when deep learning models are taken into consideration. However, the majority of publicly available datasets are of a modest size. Future study recognition must thus be based on a number of large datasets. Second, a neutral dataset needs to be employed in future research to develop models that might show better generalization performance. The generalization abilities of the updated version must be evaluated blindly on an unbiased dataset once the version has been improved via move validation. Such generalized styles will be used in hospitals for real-time diagnostics and might be of great help. Thirdly, since machine learning (ML) is a young discipline, there are still unresolved problems that require the development of fresh methodologies in order to provide effective performance.

REFERENCES

[1] Mihir Patel, Rahul Patange, Chaitanya Patil, Prof.Anuradha Kapoor. “Predicting Heart Disease Using Machine Learning Algorithm” in IRJET Volume: 09 Issue: 04|Apr 2022.

[2] Yan Fang, Jianshe Shi, Yifeng Huang, Taisheng Zeng, Yuguang Ye, Lianta Su, D axin Zhu, Jianlong Huang. “Electrocardiogram Signal Classification in the Diagnosis of Heart Diseas Based on RBF Neural Network” in Hindawi Volume 2022, Article ID 9251225.

[3] Dimitri Grun, Felix Rudolph, Nils Gumpfer, Jennifer Hannig, Laura K. Elsner, Beatrice von Jeinsen, Christian W. Hamm, Andreas Reith, Micheal Guckert and Till Keller. “Identifying Heart Failure in ECG Data with Artificial Intelligence-A Meta-Analysis” published: 25 February 2021, doi:10.3389/fdgth.2020.584555

[4] M.V.D Prasad, P. Chadvik Ram, CH. Hari Charan, V. Gopi, Sk Hasane Ahammad, Koneru Lakshmaiah Education Foundation, Guntur. “Cardiac Disease Prediction by Analysing Ecg Signal Using ML and DL Techniques.” In Nat. Volatiles & Essent. Oils, 2021;8(5): 1562 – 1566.

[5] Mamta Rani, Adutya bakshi, akhil Gupta. “Prediction of Heart Disease Using Naïve bayes and Image Processing” 2020 International Conference on Emerging Smart Computing and Informatics (ESCI) AISSMS Institute of Information Technology, Pune, India. Mar 12-14, 2020.

[6] Tanvi Dhamdhere, Sayali Bhutambare, Apeksha Bansode, Prof. Snehal Umare. “Heart Disease Dtection Using ECG Waves: A Survey” in JETIR April 2020, Volume 7, Issue 4.

[7] Ali Haider Khan, Muzammil Hussain, and Muhammad Kamran Malik. “Cardiac Disorder Classification by Electrocardiogram Sensing using Deep Neural Network” in Hindawi Complexity volume 2021, Article ID 5512243.

[8] Saira Aziz, Sajid Ahmed & Mohamed-Slim Alouini. “ECG-based machine-learning algorithms for heartbeat classification” in Scientific Reports (2011) 11:18738.

[9] “Heart diseases prediction based on ECG signals' classification using a genetic-fuzzy system and dynamical model of ECG signals” by M. H. Vafaie, Mohammad Ataei, H. R. Koofigar, November 2014, Biomedical Signal Processing and Control,14:291–296 DOI: 10.1016/j.bspc.2014.08.010.

[10] “Analysis on CBIR System for ECG Reports” by Dr. Naveen B, Mr. Raghukumar, December 2021 International Journal of Engineering and Advanced Technology 09(05):586-592.

[11] A Journal of Medical and Biological Engineering (2021) 41:422–432. “ECG Paper Record Digitization and Diagnosis Using Deep Learning” by Siddharth Mishra, Gaurav Khatwani, Rupali Patil, Darshan Sapariya, Vruddhi Shah, Darsh Parmar, Sharath Dinesh, Prathamesh Daphal, Ninad Mehendale published on 15 June 2021.

[12] Indonesian Journal of Electronics, Electromedical Engineering, and Medical Informatics (IJEEEMI) IJEEMI, Vol. 3, No. 3, August 2021, pp. 114-120 DOI: 10.35882/ijeeemi. v3i3.5 ISSN:2656-8624” Design a Monitoring Device for Heart-Attack Early Detection Based on Respiration Rate and Body Temperature Parameters” by Isna Fatimatuz Zahra, I Dewa Gede Hari Wisana, Priyambada Cahya Nugraha, Hayder J Hassaballah.

[13] Shaik Farzana, Duggineni Veeraiah. “Dynamic Heart Disease Prediction using Multi-Machine Learning Techniques” 978-1-7281-9180-5/20/$31.00 ©2020 IEEE.

[14] Pranav Madihalli, Sanket Mahajan, Aishwarya Jadhav, Saurabh Mirajkar, Rubeena A Khan, Mahesh Shinde “A Thorough Study on Heart Disease Detection through Machine Learning” E-ISSN: 2395-0056 P- ISSN: 2395-0072 VOLUME: 08 ISSUE: 04 | APR 2021.

[15] Armin Yazdani, Kasturi Dewi Varathan, Yin Kia Chiam, Asad Waqar Malik3 and Wan Azman Wan Ahmad “A novel approach for heart disease prediction using strength scores with signifcant predictors” (2021) 21:194.

[16] Senthilkumar Mohan, Chandrasegar Thirumalai, and Gautam Srivastava, “Effective Heart Disease Prediction using Hybrid Machine Learning Techniques”.

[17] Sakshi Goel, Abhinav Deep, Shilpa Srivastava, Aparna Tripathi, “Comparative Analysis of Various Techniques for Heart Disease Prediction System”.

Detection of disease using finger nail

S. Hema Priyadarshini
Department Of Medical Electronics Engineering
Dayananda Sagar College Of Engineering
Bangalore, India
priyadhema@gmail.com

Aishwarya Prabhu
Department Of Medical Electronics Engineering
Dayananda Sagar College Of Engineering
Bangalore, India
aishwaryaprabhu39.ap@gmail.com

Sahana P
Department Of Medical Electronics Engineering
Dayananda Sagar College Of Engineering
Bangalore, India
sahanap122000@gmail.com

Saritha Pal
Department Of Medical Electronics Engineering
Dayananda Sagar College Of Engineering
Bangalore, India
sarithapaldsml@gmail.com

Surabhi A S
Department Of Medical Electronics Engineering
Dayananda Sagar College Of Engineering
Bangalore, India
surabhias23@gmail.com

Abstract - In **earlier traditional systems of disease detection, doctors used to observe the nails of patients and would predict the disease. Many diseases can be identified by analyzing the nails of patients. But it is difficult for human eyes to differentiate the slight changes in color. So, it is less accurate and time-consuming. There is a need to classify diseases using nail images by applying certain image processing techniques. This project is focused on the system of image recognition on the basis of color analysis. The proposed system is based on an algorithm that automatically extracting only nails (Region of Interest). The system will process the nail image and will extract the nail's features to diagnose the disease and then the diseases are classified accordingly. Hence this proposed system can be useful in the prediction of diseases using nails. In this proposed system we are mainly focusing to classify Beau's line, yellow nail, white nail, bluish nail, and terry nail with good accuracy. To achieve this Pi camera and Google Colab are being used. The diseases can be detected in the early stage and it doesn't take much time.**

Keywords— Fingernails, Image processing, Raspberry pi.

I. INTRODUCTION

The field of medical science is extensively emerging. There are so many techniques which assist medical practitioners to diagnose patient's disease. A statistical analysis, tells us that in males themean thickness of finger nails is 0.6mm and toe nail is 1.65+0.43mm whereas in females the meanthickness of finger nail is 0.5mm and toe nail is 1.38+0.2mm. In elderly, nail surface changes dueto ageing, prominent ridges were the most common change (85%) followed by rough nails in 33%people, transverse ridges in 23% and lamellar split in 15% of people [1].

Nail is composed of laminated layers of a protein called keratin. They grow from the area at the base of the nail under the cuticle. Healthy fingernails are smooth, without pits or grooves. They'reuniform in colour, consistent and free of spots or discoloration. Usually healthy nails are pink in colour. The nail's chief function is to protect the terminal portions of the toes and fingers. On the fingers, the front edge of the nail assists in the manipulation of small objects, as well as in scratching. Fingernails play several important roles in the body such as strengthening, protection,enhancing fine motor movements and in sensation.

Transformation in nail colour and texture may indicate that the condition of health is abnormal. Nail abnormalities include symptoms such as changes in nail shape (curling or clubbing), discoloration (dark or white streaks, or other changes in colour), changes in thickness (thinning orthickening of nails), brittle nails, pitted nails, redness around nails, swelling around nails, pain around nails, bleeding around nails, nails that are separating from the skin. Possible diseases diagnosed based on the type of nails are Asthma, Heart disease, Anaemia, Iron deficiency, Zinc deficiency, Liver cirrhosis, Congestive cardiac failure, Pneumonia, Bronchitis, COPD, Hypothyroidism, Pleural effusion, bronchiectasis.

Structure of nail includes nail matrix where the nail growth occurs, nail plate which is the noticeable part of the nail, lunula which is a crescent moon contour seen at the plinth of the nail plate, Nail folds is a meagre skin furrows which hold the nail plate, cuticle a flutter thin hankie over the plinth of the nail plate and the nail assembles on the top of the nail bed.[1]. Different parameters which were chosen to detect the possible diseases includes colour, shape and texture.

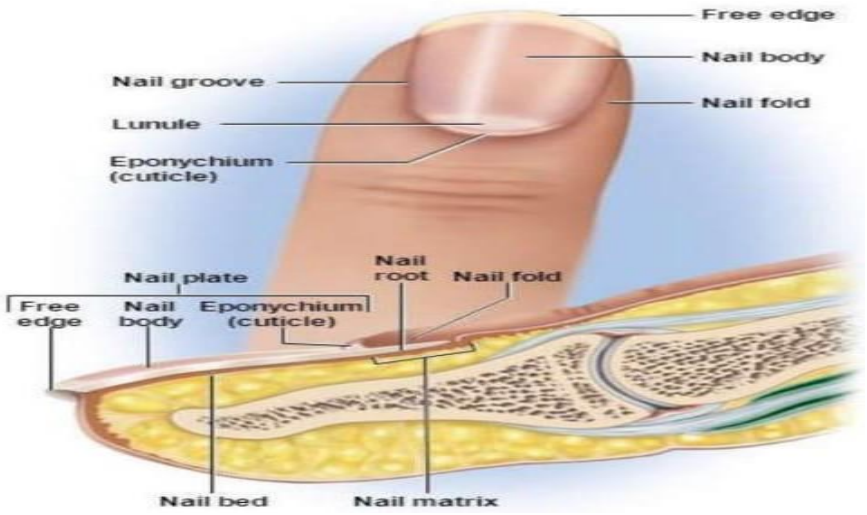

Fig 1. Structure of finger nail [1]

II. LITERATURE SURVEY

This paper deals with the finger nail analysis, in which the color, shape and texture plays a vital role in diagnosing the patients' health status. The proposed method extracts the nail from the finger and compares the segmented nail with the healthy nail. If it finds any deviation in color, shape or texture, then the patient can be concluded that he is unhealthy. In future RGB model can be used to identify the color of the nail and identify the disease for the further treatment [1]. In this paper they analyzed the human's hand nail for diagnosing diseases at early stage. The nail color change is used for diagnosis purpose. Using Weka tool, the training data set is prepared from the nail images of patients of particular disease. The disease is diagnosed by comparing the extracted feature with the training data set. The results showed that the color feature of nail image is suitably matched with the training data set [3]. This paper have proposed a study on eye difficulty using palm print and image processing technique they select a region of interest for prediction of disease from image, then apply sobel filter for noise reduction and canny algorithm to detect edges and lines [5]. In this paper they have proposed a computerized binarisation technique to analyze NC images. It extracts the skeletons of the capillaries by Difference-of-Gaussian approach and thresholding based segmentation. Then, Post processing step removes smaller image artefacts [8]. This paper have done the analysis of nail color model to predict the diseases. In this model, human palm nail color is observed for the prediction of probable diseases. The performance of the model provides accurate results and it overcomes the limitations of human eye like subjectivity and resolution power [9].

III. METHODOLOGY

The proposed system that is being developed is focused on image recognition based on color analysis. In healthcare field, study of human nail has its own significance. Many diseases can be diagnosed by scrutinizing nails of the hand, as human eyes have limitation in distinction in color.This will automatically extract nail area and scrutinize the nail part for disease detection based oncolor of nail. Here, first training data set is prepared from nail images of patients of specific diseases. For classification average of red, green and blue color is calculated. During matching phase, RGB average is calculated for input image and then matched with training set data. Throughthis system we can analyze diseases such as zinc deficiency, Bronchitis, Anaemia, Asthma, Cirrhosis of liver.

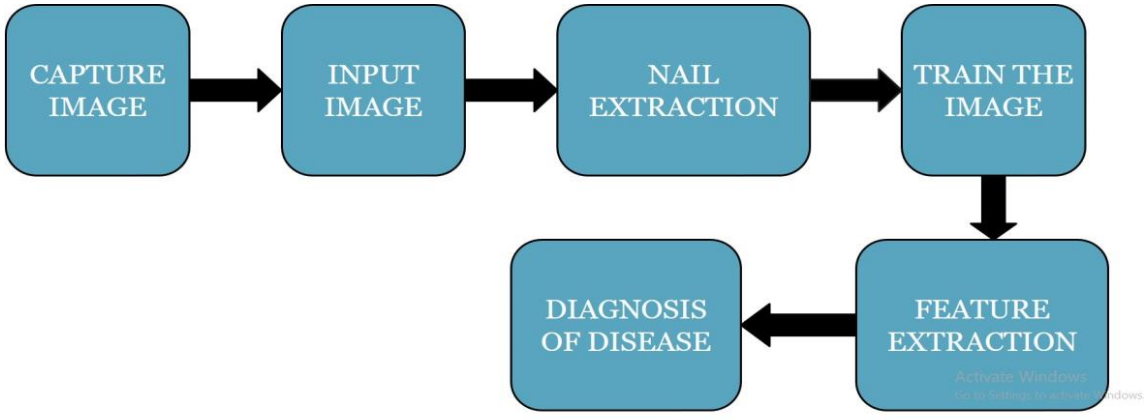

Fig 2. Block Diagram

The Proposed Model has five major steps:

Capture the image: the nail image to be diagnosed is captured using pi camera 5MP. Then captured image is resized to be at least 224x224 and then cropping from the center.
Input to the model: The image is stored in PNG form in raspberry pi OS. Scanning the image containing fingers, back side of palm region in appropriate brightness.
Extraction of the cropped Nail region from the entire Palm: Applying segmentation method on the image to extract the nails region from the entire image.
Train the image: The segmented nail image is now being processed on the basis of colorand texture and we will determine the health of the nail by comparing the segmented image with the dataset present.
Disease Prediction using Knowledge base: The result will be generated on the basis of analysis and the disease would be predicted if present.

A. Hardware Methodology

Raspberry pi and Camera module are interfaced and the images are captured from the camera and are stored in raspberry pi OS. The nail images are sent to the PC via Bluetooth. These images are downloaded into the system and the possible diseases are predicted through google Colab.

Data Input Constraints:

Nails should be clean, having no any color like nail polish or any artificial marks on nails.
Image should be taken under conditions like proper sunlight.
Image background should be white or black background.
Image should be taken without flash and clear.

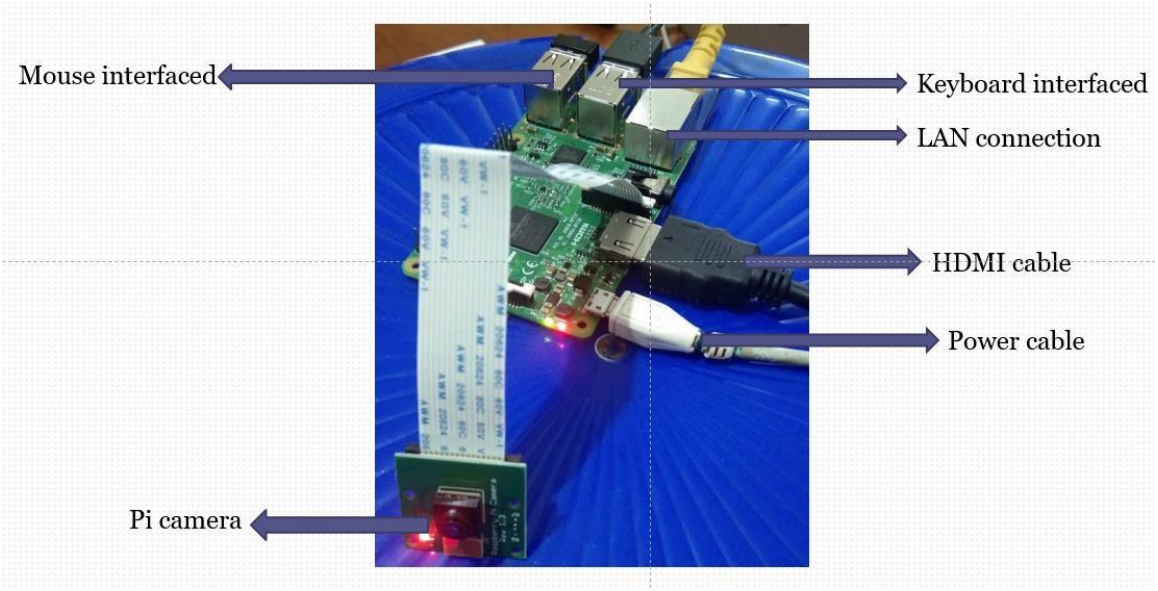

Fig 3. Hardware Connection

B. Software Methodology

a) Load the model
In order to load the model, we use the load model() function specified in the keras.models library. we will first have to import this function from the relevant libraryin order to use it. The user will specify the name and location of the file with an .h5 extension. the syntax is given below from keras.models import load_model model_new = load_model("myMode 1.h5").

b) Create the array
Then we create the array of the right shape to feed into the keras model The 'length' or number of images we put into the array is determined by the first position in the shape tuple, in this case it is 1.

c) Convert image to RGB
RGB color model is a color model in which the three primary colors i.e., red, green, blue are mixed with each other to produce an Array of colors. The name of the model (RGB) is based on the initials of the three primary colors red, green, and blue. The main motive of the RGB model is representation of images in electronic equipments, such as televisions and

computers, it has also been used in traditional photography. Getting the RGB values of an image returns a tuple of the red, green, and blue values.

d) Resizing the image

Most of the digital image is a two dimensional plane of pixels and it has a width and height. The Image module from pillow library has an attribute size. This tuple consists of width and height of the image as its elements. To resize an image, we call the resize() method of pillow's image class by giving width and height.

e) Turn the image into a numpy array

A numpy array is a grid of values, all of the same type, and is indexed by a tuple of nonnegative integers. The number of dimensions is the rank of the array; the shape of an array is a tuple of integers giving the size of the array along each dimension.

f) Run the inference

Inference is concerned with the calculation of posterior probabilities based on one or more data observations. We use Pre trained model to make predictions against previously unseen data. So, when a new unknown data set is input through a trained model, it outputs a prediction based on predictive accuracy of the model.

g) Reverse mapping

The database also includes zone files that use the IP address as a key to find the host name of the machine, enabling IP address to host name resolution. This process is called reverse resolution or more commonly, reverse mapping. Reverse mapping is used 10 primarily to verify the identity of the machine that sent a message or to authorize remote operations on a local host.

h) Prediction of diseases

The result will be generated on the basis of analysis and the disease would be predicted if present. If no parameters are detected, then the person is declared as HEALTHY with no symptoms.

I. RESULTS AND DISCUSSION

There are five main parts of nail namely lunula, cuticle, nail root, nail plate, nail lines out of which we used nail plate. In presented system, system analyses the human nail and gives probable disease for person including healthy case. Here, for disease prediction nail color (average rgb) value used as a nail feature. This model gives more accurate results than human vision, because it overcomes the limitations of human eye like subjectivity and resolution power.

Case 1: Abnormal nail given as input.

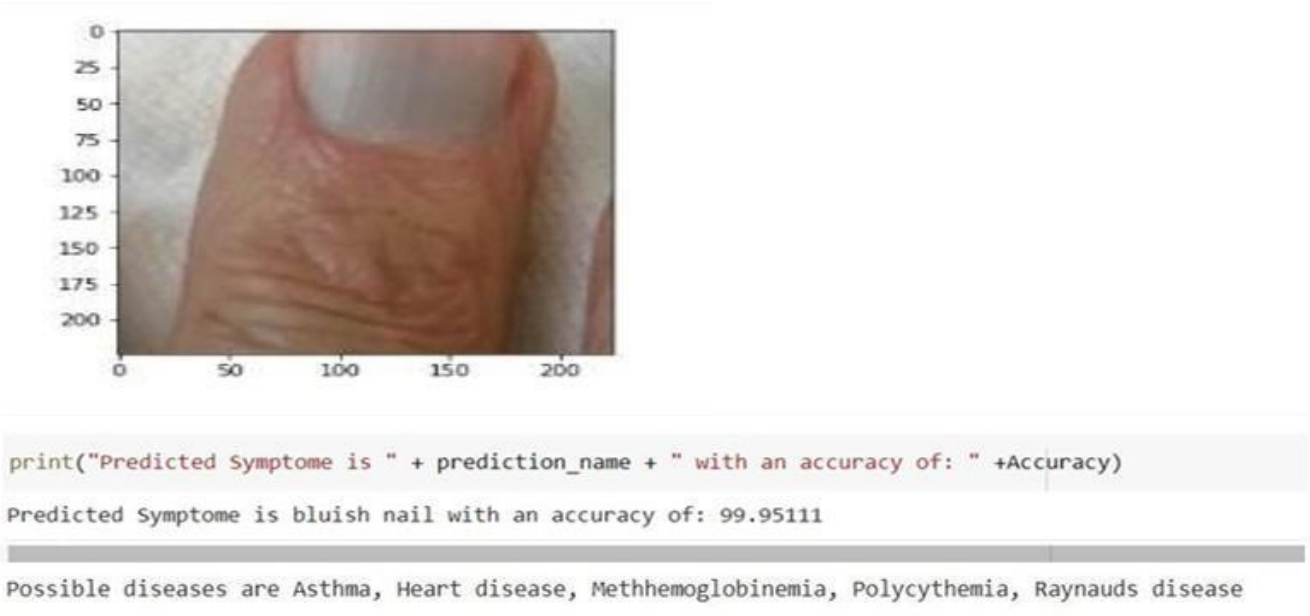

Fig 4. Abnormal Nail input

Prediction Accuracy is calculated using the formula, Accuracy=str(np.max(result*100)).

In this case accuracy predicted is 99.95, classified as Bluish Nail.

Predicted diseases are Asthma, Heart disease, Methhemoglobinemia, Polycythemia,Raynauds disease.

Case 2: Normal Nail given as imput

Fig 5. Normal Nail Input

II. CONCLUSION

Health is a critical aspect for Human life. Identification of human health conditions and accurately predicting the symptoms of the diseases is useful work for the society.Machines are made by man to make their lives easier and better. To solve problems whichare beyond the capability of the humans and it is evident from the fact that the disease inthe nail can be diagnosed easily. For these a new system is designed based on Digital Image Processing and nail-color analysis. Nail colors are used for the disease detection. It helps in recognizing disease of the person and minimizes the cost of the diagnosis of diseases.

This system analyzes the human nail and gives probable disease for person including healthy case. Here, for disease prediction nail color (average RGB) value used as a nail feature. This model gives more accurate results than human vision, because it overcomesthe limitations of human eye like subjectivity and resolution power. This detection systemmakes easy for doctors to give correct treatment to patients. Using this algorithm, the computer system would be able to predict some specific diseases which could beidentified by observing nails. Hence, this system can be useful in healthcare domain, especially in routine check-ups. So, the diseases could be able to get caught in their initialstages.

IV. REFERENCES

[1] Dr A Rani Chitra, “Finger Nail Analysis to Diagnosis the Disease – A Study”, International Journal of Management, Technology and Engineering, Volume 8, IssueX, OCTOBER/2018, Page No:2039.

[2] Kumuda S., “An Image Pre-processing Method for Fingernail Segmentation”, IEEE2nd International Conference on Signal and Image Processing, 2017; 978-1-5386- 0969- 9/17.

[3] Trupti S Indi, Yogesh A Gunge, “Early-Stage Disease Diagnosis System Using Human Nail Image Processing”, International Journal of Information Technology and Computer Science, 2016, 7, pp 30-35.

[4] Sukhdeep Kaur, Manjit Sandhu, Jaipreet Kaur, “Analysis of Various Image Segmentation Techniques Using MATLAB”, International Journal of Advanced Research in Computer Science and Software Engineering, Volume 6, Issue 3, March 2016, ISSN: 2277 128X, pp. 836-841.

[5] Indrakumar S S, Dr. M S Shashidhara, “Study on Eye Troubles Using Palm Print And Image Processing Technique”, International Journal Of Recent Trends In Engineering & Research (Ijrter), Volume 02, Issue 05, May – 2016; Pp. 198-201.

[6] V Sharma, A Shrivastava, “System for Disease detection by analyzing finger nails Color and Texture”, International Journal of Advanced Engineering Research and Science (IJAERS) Vol-2, Issue-10, Oct- 2015, ISSN: 2349-6495, pp.1- 6.

[7] Nityash Bajpai, Rohit Alawadhi, Anuradha Thakare, Swati Avhad, Sneha Gandhat, “Automated Prediction System For Various Health Conditions By Analysing Human Palms And Nails Using Image Matching Technique”, International Journal of Scientific & Engineering Research, Volume 6, Issue 10, October-2015, ISSN 2229-5518, pp.609-613.

[8] Doshi, N.P, Schaefer, G, Shao Ying Zhu, “An Improved Binarisation Algorithm forNailfold Capillary Skeleton Extraction”, IEEE Xplore, SMC, 2013; pg. 2565 – 2569.

[9] HardikPandit, Dipti Shah, "The Model of nail color analysis – An application of Digital Image Processing", International Journal of Advanced Research in ComputerScience and Software Engineering, Volume 3, Issue 5, pp. May 2013, ISSN: 2277 128X.
[10] A. Tsuda, S. Ueno and S. Sakazawa, "A method for extraction of nail area under varying luminance for the 3D nail art system on mobile phones", IEICE Tech. Committee. PRMU 110 (2011), 381-–364.

Instruction to Authors

Papers dealing with original research work of basic as well as applied, Biomedical device, Instrumentation, Biomaterial and Tissue engineering, Medical Imaging, Bio mechanic, Rehabilitation, Medical Information, AI and Big Data incorporating new ideas and concepts, novel developments of experimental/ practical significance and theoretical work dealing with aspects of Bio-medical and Life Science Engineering Journal. Review/Tutorial Papers describing the state of art of any particular topic/areas of Bio-medical Engineering are also welcome.

Manuscript Preparation

1. Manuscript should be type written and double spaced single column with adequate margins.
2. The abstract should reflect / highlight the reported work and should not more than 200 words.
3. The Cover page should contain the title, author's name, affiliationand mailing address. A separate list of figure caption should be marked clearly on each illustration.
4. Original Illustration in Indian Ink/Photographs must be sent to the Editor upon receipt of acceptance of the manuscript for publication in the journal.
5. Reference should appear in a separate reference section at the end of the paper with items referred to be numerals in square brackets.References must be complete in all aspects-author's name, title, periodical, volume, inclusive page numbers, month, year etc.

Submission of Manuscript:

1. Authors should submit three copies of the manuscript each complete with abstract, reference and illustration to the Editor of the journal.
2. The Editor upon receipt of manuscript acknowledges the author and will complete the review process. The Editor then communicates to the author, the decision concerning the manuscript.

Biomedical Engineering Society of India

Website: www.Bmesi.org.in

The Biomedical Engineering Society of India is an Organization with members having principal professional interest in Biomedical Engineering. Members from academic institution, R &D organizations, biomedical industry and individuals with sufficient interest in biomedical engineering are eligible for membership in the society upon payment of suitable membership fee (individual life membership Rs. 1520/, Institutional life membership Rs 15200/.

Published By

Dr. G Muralidhar Bairy, Secretary BMESI

Printed By

Manipal Press Ltd., Manipal - 576104

Journal of
Biomedical Engineering
Society of India